UNIVERSITY OF GHANA

COLLEGE OF BASIC AND APPLIED SCIENCES

EFFECTS OF TISSUE HETEROGENEITIES ON DOSE ESTIMATION IN BRACHYTHERAPY.

BY

KWARFO GORDON

(11004511)

THIS THESIS IS SUBMITTED TO THE UNIVERSITY OF GHANA, LEGON IN PARTIAL FULFILMENT OF THE REQUIREMENT FOR THE AWARD OF MASTER OF PHILOSOPHY (MPHIL) MEDICAL PHYSICS DEGREE.

DEPARTMENT OF MEDICAL PHYSICS,

SCHOOL OF NUCLEAR AND ALLIED SCIENCES

NOVEMBER, 2024

DECLARATION

I declare that this thesis work is the result of my own research and does not contain any information that has been previously published by another person or submitted for the award of any other degree elsewhere, the exception of any places where other people's work is referenced.

.....

.....

KWARFO GORDON

(STUDENT)

DATE: 4/11/2025

DR. SAMUEL NII ADU TAGOE

(PRINCIPAL SUPERVISOR)

DATE: 9/11/2025

.....

DR. MARK POKOO-AIKINS

(CO-SUPERVISOR)

DATE: 10/11/2025

DEDICATION

This thesis work is dedicated to Mr. Emmanuel Kwasi Nketiah (Nawho) of blessed memory and Madam Charity Kyeraa Diawuo (Afia Nawho) as well as to the memory of my brother, Mr. Arko Joshua.

ACKNOWLEDGEMENT

All praise and thanksgiving go to God Almighty for showing me His endless goodness, grace, love, guidance and protection during the entire period of this research work. I would like to express my heartfelt and sincere appreciation to my supervisors, Dr. Samuel Nii Adu Tagoe and Dr. Mark Pokoo-Aikins, for their selfless and invaluable direction, recommendations, motivation, and assistance in conducting this study and putting together this thesis. I also want to convey my gratitude to all the medical physicists who in one way or the other helped on this project, as well as the National Radiotherapy, Oncology and Nuclear Medicine Center (NRONMC) personnel and staff.

I would like to express my sincere appreciation to all my lecturers, colleagues, and students in the Department of Physics, School of Nuclear and Allied Sciences, for their various contributions and support. Special thanks also go to my mother, Madam Mary Somea, my siblings and most especially, Ruth Henewaa for their advice, support and love they showed me during this period of study.

TABLE OF CONTENT

LIST OF FIGURES

LIST OF TABLES

LIST OF ABREVIATION

AAM	Analytical Anisotropic Method
AAPM	Association of American Physicists in Medicine
BRT	Brachytherapy
CCC	Collapsed Cone Convolution Superpositions
CRS	Computerized Imaging Reference Systems
CT	Computed Tomography
CVA	Cerebrovascular Accident
D	Dimensional
DC	Drive Check
Dcal	Dose calculated
Dmeas	Dose Measured
EBRT	External Beam Radiotherapy
EDP	Electron Density Phantom
EDW	Electron Density of Water
Gy	Gray
HDR	High Dose Rate
HU	Hounsfield Units
IBA	Ion Beam Applications

ICRU	International Committee for Radiological Units
IGRT	Image-Guided Radiotherapy
IMRT	Intensity-Modulated Radiation Therapy
KVP	Kilo Voltage Peak
LDR	Low Dose Rate
MC	Monte Carlo
Mcor	Mean Corrected
MDR	Medium Dose Rate
MRI	Magnetic Resonance Imaging
NaOH	Sodium Hydroxide
nC	Nano Coulombs
NRONMC	National Radiotherapy Oncology and Nuclear Medicine Center
OAR	Organ At Risk
PDR	Pulsed Dose Rate
PET	Pet Emission Tomography
PSFs	Point Spread Functions
QA	Quality Assurance
QC	Quality Control

R^2	Regression
rED	Relative Electron Density
ROI	Region Of Interest
SAE	Society of Automotive Engineers
SPI	Source Position Indicator
TG	Task Group
TPS	Treatment Planning Systems
UGMC	University of Ghana Medical Center
ULDR	Ultra Low Dose Rate
VMAT	Volumetric-Modulated Arc Therapy
W	Winter
WL	Window Level
WW	Window Width

ABSTRACT

This study investigated the impact of tissue heterogeneities on dose estimation during brachytherapy treatments. Variations in tissue densities can significantly influence dose distribution, potentially affecting treatment efficacy and patient outcomes. The research was conducted at the National Radiotherapy Oncology and Nuclear Medicine Centre (NRONMC) at Korle Bu Teaching Hospital, Accra, Ghana. A Perspex phantom was fabricated to replicate the human body, and materials such as NaOH, Frytol vegetable oil, Quartz Total (SAE15W-40) engine oil, and air were used to simulate various human tissues, including liver, muscle, adipose, and lungs (exhaled). The results revealed discrepancies between the dose calculated by the treatment planning system (TPS) and the measured dose, suggesting that the actual dose received by the tumor can be influenced by tissue heterogeneities. The percentage dose differences, which ranges from -34% to 2.10% in summary, highlighted the significant role of tissue density and positioning in shaping dose distribution during brachytherapy. While the study demonstrates the importance of accounting for tissue heterogeneities, the limited range of materials used to mimic human tissues represents a limitation, suggesting the need for further research with a broader variety of tissue-equivalent materials. These findings emphasize the necessity of incorporating tissue density variations into dose calculations for more accurate brachytherapy treatment planning.

CHAPTER ONE

INTRODUCTION

1.0 BACKGROUND OF THE STUDY

Chargari et al. (2019) explained radiotherapy as a targeted approach that can be used in treating cancer and can be done through brachytherapy, teletherapy, or a combination of both approaches. The main objective for radiation treatment is to deliver the highest dose possible to malignant tissue while limiting the dose to healthy tissues.

According to Chargari et al. (2019), brachytherapy is a method of cancer treatment that involves the placement of radiation sources near the tumor. This can be achieved through intracavitary therapy or interstitial implantation. When brachytherapy is used instead of teletherapy, the dose homogeneity in the target volume is higher (Jamadagni et al., 2024). The tumor type determines the type of radioisotope to use as the brachytherapy source. Brachytherapy is a local treatment and treats only a specific part of the body. It is often used to treat cancers of the head and neck, breast, cervix, prostate, and eye (Deng et al., 2017)

Cobalt-60 (Co-60) is a radioisotope that has a half-life of 5.27 years. The use of cobalt-60 sources in high dose rate (HDR) remote afterloading brachytherapy is still relevant despite the larger size of earlier versions. Currently, there are cobalt - 60 sources that are small and have geometrical dimensions compared with earlier versions.

A new technique that uses a miniature Co-60 source is gaining a lot of relevance because, Co-60 sources have the advantage of having a longer half-life (5.27 years), which means it

needs to be replaced roughly every 5 years (Oh et al., 2023). Another substantial advantage of cobalt-60 is the reduction of the number of resources needed for the transportation of radioactive sources into other countries, changing and disposing of the sources, meeting quality assurance regulations and providing financial and logistical savings (Healy et al., 2016)

Currently, the required amount of dose is measured using the procedures or protocols proposed in 1995 by the American Association of Physicists in Medicine (AAPM, TG43) in brachytherapy. The measurement of the dose is done in a homogeneous water phantom, which is frequently used to determine the required dose for brachytherapy treatments (Zabihzadeh et al., 2013). In recent years, several algorithms such as TG-43 Formalism (AAPM Task Group 43), TG-186 Model-Based Algorithms, Monte Carlo Algorithm have been developed to influence the dose distributions in brachytherapy. These algorithms and existing protocols encompass analytical methods as well as those utilizing the Monte Carlo (MC) code.

According to Zabihzadeh et al. (2013), the limitation of the TG-43 protocols as proposed by AAPM is that it does not take into account the impact of tissue heterogeneities, such as bone, muscles, liver etc., on dose distribution. The application of TG-43 protocol dosimetry data, which assumes equality of water and different tissues not withstanding heterogeneities, weakening and scattering effects, may result in inaccuracies in dose estimations for tissues in treatment planning systems (TPS).

Cancer is a generic term for a large group of diseases that can affect any part of the body. Other terms used are malignant tumours and neoplasms. One defining feature of cancer is

the rapid creation of abnormal cells that grow beyond usual boundaries, and which can then invade adjoining parts of the body and spread to other organs with the latter process, referred to as metastasis. Widespread metastases are the primary cause of death from cancer. (Brown et al., 2023). Factors such as adipose tissue (fats), muscles, bones and organs make the human body heterogeneous according to tissue heterogeneities leading to variations in tissue densities. The variations in the tissue densities have great effects on the distribution of radiation dose within the body and influence the accuracy of the dose distribution (Morrill et al., 1994).

Modern radiotherapy planning systems rely on simulation and medical images to create detailed patient geometry and internal structures. Additionally, these systems incorporate methods for heterogeneity correction, allowing for the consideration of variations in tissue density when assessing dose distribution (Glide-Hurst & Chetty, 2014).

This research work uses Phantom to analyze the effects of tissue heterogeneity by using tissue-equivalent materials. The high dose rate (HDR), with its unit given as Gray per hour (Gy/h) for afterloader at the National Radiotherapy center, Korle-bu teaching with Cobalt 60 source as its radioisotope was used in this study. The measured dose values of the selected materials and the TPS calculated dose were compared to ascertain the discrepancies that occurs between them during brachytherapy treatment.

1.1 STATEMENT OF THE PROBLEM

In Brachytherapy, predicting accurately the distribution of radiation dose within inhomogeneous tissues remains one of the challenges. Tissue heterogeneities can alter the scattering and absorption of the radiation beam which affects the deposition of dose.

Current algorithms dedicated to treatment planning systems (TPS) assumes that; tissues are homogeneous which might result in significant dosimetry inaccuracies by patients undergoing Brachytherapy procedures and as such, there is the need to ascertain the levels of inaccuracies and the risk of exposure of radiations to patients during brachytherapy procedures.

1.2 GENERAL OBJECTIVE OF THE RESEARCH

To investigate and ascertain the influence the deposition of dose during HDR brachytherapy treatment as a result of variations in tissue densities.

1.2.1 SPECIFIC OBJECTIVES

1. To design and construct a phantom with compartments that are adequate to hold the materials selected for irradiation.

2. Investigate how varying tissue types affect the dose distribution in brachytherapy applications.

3. To evaluate TPS calculated dose and measured doses in heterogeneous medium.

4. To develop semi empirical equation to convert TPS calculated dose to measured dose such that, the effects of inhomogeneities can be accounted for.

1.3 RELEVANCE AND JUSTIFICATION

The human body is heterogeneous (made of different tissues), which may affect dose distribution to patients going through brachytherapy treatment because of variations in their densities. According Ravikumar and Lakshminarayana (2012), Morden treatment planning systems (TPS) dedicated to brachytherapy assumes all tissues as homogeneous and as a result, do not account for heterogeneities.

Due to the above effects, it is very important for this research to be done to help account for the inaccuracies of heterogeneities in brachytherapy which will help to improve the accuracy of radiation delivery to tumours and enhances patient safety since it influences clinician choice of dose and exposure to healthy tissues.

1.4 SCOPE AND LIMITATION.

The scope of this work is to investigate and ascertain the influence the deposition of dose during HDR brachytherapy treatment as a result of variations in tissue densities. This research work was done at the National Radiotherapy Oncology and Nuclear Medicine center (NRONM), Korle-bu Teaching Hospital in Ghana and specifically under the brachytherapy unit.

The study examined the extent to which tissue heterogeneities affect the accuracy of dose distribution in brachytherapy and some ways to improve the treatment outcomes was suggested. The study was limited by the scope of the research question and the time and resources available.

1.5 ORGANIZATION OF THE RESEARCH

There are five chapters in this research work. The first chapter sets the study's context, formulates the problem statement, outlines the general and the specific objectives, and also defines the study's parameters. In order to provide a thorough understanding of the topic, chapter two dives into an in-depth analysis of existing literatures. This chapter covers the theoretical underpinnings, as well as a number of concepts and empirical research carried out by other authorities. The third chapter accounts for the materials and methodologies utilized throughout the investigation, culminating in the simulation and validation of the procedures, guaranteeing the excellence, dependability, and efficacy of the current protocols. This chapter also covers the development and validation of an improved protocols. The research study's findings are presented in details in Chapter Four, along with a discussion of their applicability and validity. Lastly, Chapter Five offers recommendations and findings derived from the study outcomes.

CHAPTER TWO

LITERATURE REVIEW

2.0 OVERVIEW

This chapter provides a thorough review of the literature regarding tissue inhomogeneity.

2.1 INTRODUCTION TO BRACHYTHERAPY

Brachytherapy is a kind of radiation therapy used for treating lesions/cancer. Henri Becquerel discovered radioactivity in 1896 and shortly after this discovery, Pierre Curie and Alexander Graham Bell independently concluded in the early 1900s that placing a radioactive source directly into or beside a tumor can cause it to shrink (Chargari et al., 2019). This discovery led to the realization that radiation can be an effective treatment for malignant tumors.

It is a targeted radiation therapy used to treat cancer and this method involves placing a sealed radioactive source directly into or near the tumor, either directly or by using catheters. Since the early 1900s, brachytherapy has been a common treatment option when contact brachytherapy was developed (Holschneider et al., 2019).

According to research conducted by Williamson et al. (2021), The use of brachytherapy in cancer treatment has steadily increased, establishing it as the standard of care either as a standalone treatment or as an additional boost following external beam radiotherapy (EBRT) for tumors that require a high radiation dose to achieve a cure. Since its inception in the 20th century, brachytherapy has become an optimal tool within radiation therapy. As of 2019, it involves a wide range of medical specialties, both in the referral to and the placement of brachytherapy (Chargari et al., 2019)

2.1.1. PRINCIPLES OF BRACHYTHERAPY

The localized radiation principle is an important concept to reduce radiation damage to surrounding healthy tissues. Radiation therapy, another name for local treatment, is extremely focused on the precise body part that is being irradiated. Compared to external beam therapy, brachytherapy allows for a larger dosage in a smaller area by delivering radiation directly to the treatment site (Gregoire et al., 2020).

As highlighted by Nikolayev et al. (2019), the principle of implant uses a radiation source which is most often, sealed in a holder brachytherapy which is an internal radiation therapy permits or allows a higher dose of radiation which is focused on a small area that might be treated with external radiation. The types of implants which include pellets, seeds, ribbons, wires, needles, capsules, balloons, or tubes are placed in the body, either close to or inside the tumor and it helps to reduce the effect of radiation harm on a very few normal cells as possible (Mariotti) 2021

According to Davé et al. (2016), positioning the implant is mostly done in an operating room that is specially built to ensure that, the radiations are well shielded. The patient is placed on anesthesia while undergoing the procedure, Applicators, usually metal or plastic tubes may contain one or more implants which are kept in the body cavity or tissue. Imaging which is an essential part of the procedure such as X-rays, ultrasound, MRI, or CT scan to locate the exact place the implant needs to be positioned. The health professionals handling the implants always wear special gear that protects them from exposure once the implants are taken out of the container (Dupoiron et al., 2020).

Implants are temporary or permanent depending on how long it is left in the body. This simply implies that some implants are permanent, while others are taken out after a few

minutes or days which is a temporal implant as indicated by Alberga et al. (2020). The type of cancer and where it is situated in the body, the general health and treatments that one has had will generally influence the type of implants to be applied (Ether & Nguyen. 2018).

Temporary implants are commonly used for various cancers, such as head and neck, cervical, and endometrial cancers. For the permanent implants, the radioactive source is continuously emitting over a period. It is commonly used for prostate cancer (Pignol et al., 2015).

High-dose-rate (HDR) brachytherapy principle, delivers a higher dose of radiation through applicators at a fast rate to the targeted tissue. Treatment is relatively shorter, which takes a few minutes and, in some instances, can be repeated twice a day over a few days or weeks (Morton et al.,2020).

In the case of Low Dose Rate (LDR) Brachytherapy, the implant emits a lower dose of radiation over a longer time frame and some implants are kept in the patient's body for a few days before being removed. This may cause the patient to be hospitalized and preferably or sometimes in a special/isolated room during treatment. Patients with larger implants might have to stay in bed and lie still to prevent the implants from moving. Some smaller implants (such as the seeds or pellets) are placed permanently and over some weeks, the source becomes inactive and does not emit radiation. The seeds or pellets are about the size of rice grains and rarely cause problems (Stish et al.,2018).

2.1.2. TYPES OF BRACHYTHERAPY TECHNIQUES

There are several classifications or types depending on the need, one of the types of brachytherapy techniques is by the duration of the irradiation: This type of technique emphasizes that there are two different types of brachytherapy which is the permanent type of brachytherapy is when the seeds (radioactive sources, radionuclides, isotopes) remain inside the body, and the temporary type of brachytherapy, which indicates that, the isotopes are inserted into a tumor or near the tumor inside the body, and then removed as highlighted by Takácsi-Nagy et al. (2017).

It can also be classified according to how the radionuclide is positioned: Interstitial brachytherapy which involves the radioactive sources that are been placed inside the tumor and Contact brachytherapy or Plesio brachytherapy is when the radioactive sources are placed close to the tumor. The four different kinds of contact brachytherapy include intracavitary brachytherapy, intraluminal brachytherapy, endovascular brachytherapy, and surface brachytherapy. (Prisciandaro et al.,2020).

The final classification of the brachytherapy technique is by the dose rate and the ICRU definition of the dose rate is systems have a dose range between 0.4-2.0 Gy/h and provides adequate protection against radiation, it does not give designers as much creative freedom as higher dose rate sources that have stepping positions and dwell lengths that may be adjusted however it is not used in many nations now. One radiation therapy that has been used for almost a decade to treat localized prostate cancer is low-dose-rate brachytherapy according to King et al. (2021). As stated by Berg et al. (2019), the primary goal of this technique is to assist in inserting a tiny radioactive seed into the prostate gland to act as a direct radiation source and is administered as a monotherapy in addition to serving as a

boost when combined with external beam radiation therapy (EBRT), but not as a palliative measure.

With high-dose-rate brachytherapy, a radioactive source is inserted into the cancer tumor through an applicator and this kind of patient treatment takes a few minutes before the source is removed. The cancer is treated with a high radiation dosage but the healthy surrounding organs are mostly spared. This can be carried out once a day for a few weeks, or twice a day for a few days. The radioactive material is not kept permanently in the body and the applicator may be inserted before each treatment, or it may be kept in place in between treatments. High-dose-rate (HDR) has a dose range above 12 Gy/h (> 12 Gy/h) (Åström et al.,2018).

Another more contemporary brachytherapy modality called pulsed-dose-rate (PDR) uses a combination of the radiobiological benefits of brachytherapy (repair advantages) with the physical benefits of technology (isodose optimization, planning flexibility, and radiation safety). Pulse-dose-rate ranges between 0.5-1.0 Gy/h according to Balgobind et al. (2015).

Medium-dose-rate (MDR) has a dose range between 2-12 Gy/h and the dosage is typically administered in MDR brachytherapy at a rate of 2 – 12 Gy/h (+/−10 Gy/h) using cesium-137 sources in 1-3 fractions, depending on the dose. The after-loading treatment might be either automatic or manual. Compared to LDR treatments, the overall dose must be decreased because of the high dose rate. Mostly, the patient is allowed to stay in the hospital throughout the treatment period. Gynecologic malignancies are the most common site of application; however, it is rarely utilized (Gill et al.,2015).

Ultra LDR (seeds, permanent implants) BRT is defined within a range of 0.01-0.3 Gy/h. Permanent implants such as ^{125}I, ^{103}Pd, and ^{131}Cs are mostly used in Ultra Low Dose Rate (ULDR) BRT. Approximately, a 7 – 21 cGy/h dose rate of implants is enough to start with during this type of treatment. Ninety-nine per cent of the complete dosage of ^{103}Pd is administered in 56 days, and ninety per cent of the total dose of ^{125}I is administered in 197 days. Thoracic tumors and prostate cancer are the two conditions for which ULDR BRT is most frequently utilized. For prostate cancer patients, the ^{103}Pd and ^{125}I permanent ULDR BRT seed implants yield comparable outcomes in terms of toxicity and disease management. As a result of the high dose rate, ^{103}Pd may be more efficient in dedifferentiated tumors as indicated by Moran et al. (2021).

According to Sebesta and Anderson (2017), ULDR BRT typically does not require an extended treatment period, often only needing one night at the treatment facility. This method is less invasive compared to prostatectomy. Other advantages include the fact that the treatment is performed just once, eliminating the need for repeat procedures, and it poses minimal risks to surrounding normal tissues, such as the rectum, bladder, and urethra. Additionally, it better preserves erectile function.

Some common challenges associated with ULDR BRT are that it requires anesthetic and surgical procedures, is expensive and causes temporal changes in the patient's lifestyle as a result of the radioactive implant. It can also lead to adverse effects in the urine that only last for a few weeks or months. It is not accessible in all treatment centers (Ferranti et al.,2020).

2.1.3. IMPORTANCE OF ACCURATE DOSE ESTIMATION

Accurate dose estimation ensures patient safety. Precise dose calculation is essential in healthcare delivery to guarantee patient safety. When radiation doses are administered in error, it may lead to underdosing which may reduce the efficacy of treatment, and overdosing may result in serious side effects such as tissue necrosis and reduced organ function. Precise dosage calculation lowers the risk of injury and ensures that patients have secure and efficient medical care (Cicero et al., 2020)

When doses are accurately estimated, it helps to achieve treatment efficacy. The main objective of brachytherapy is to minimize damage to the surrounding healthy tissues while precisely administering a radiation dose to the target location. The probability of treatment success is increased when the intended target receives the recommended radiation dose, which is ensured by accurate dose estimation (Xiang et al.,2015).

Accurate dose estimation leads to treatment Planning optimization. In brachytherapy, precise dosage calculation is essential to treatment planning. To obtain the required radiation dose distribution inside the target volume while avoiding exposure to healthy tissues, radiation oncologists might use it to optimize the placement of radioactive sources and modify treatment parameters. This modification can lessen the need for retreatment and enhance treatment outcomes (Han et al.,2014)

Accurate dose estimation helps in the minimization of side effects. Accurate dose estimation aids in reducing the possibility of negative effects of radiation-related side effects, many drugs and therapies by precisely assessing the dosage. This is especially crucial for brachytherapy, which involves putting radiation sources inside or next to the

tumor. By protecting neighboring healthy tissues and organs, precise dosimetry lowers the risk of side effects like radiation burns or organ dysfunction.

Accurate dose estimation is a cornerstone of quality assurance in brachytherapy. It involves rigorous verification processes, including dosimetry measurements and treatment plan verification, to confirm that the intended dose is delivered as planned. This helps in maintaining the highest standards of patient care and treatment quality (Fonseca et al.,2020).

2.2 DEFINITION AND TYPES OF TISSUE HETEROGENEITIES.

Differences in the makeup and density of various bodily tissues are referred to as tissue heterogeneities. These discrepancies may result from the existence of air cavities, implants, or other foreign materials, as well as changes in tissue types, including fat, muscle, and bone. Tissue heterogeneities make it difficult to precisely estimate and administer the radiation dose to the tumor while protecting nearby healthy tissues according to Wei et al. (2021).

2.2.1 TYPES OF TISSUE HETEROGENEITIES

Differences in tissue composition and density can give rise to tissue heterogeneities in brachytherapy. Khosroabadi et al. (2016) identified the following as some typical tissue heterogeneities that arise during brachytherapy. Bone is one of the tissues that makes the human body heterogeneous but compared to soft tissues, bone tissue has a higher density and atomic composition. The distribution of radiation dose can be significantly altered by the presence of bone close to the treatment site.

In comparison to the surrounding tissues, air cavities, such as those found in the lungs or gastrointestinal tract, have a very low density. Calculations and delivery of doses might become very unclear when air is present. Also, metallic implants and prosthetic materials, such as dental fillings or hip replacements, might bring differences in composition and density that can cause dose perturbations.

The density of adipose tissue, sometimes known as fat, differs from that of other tissues. Changes in the distribution of fat can affect the distribution of doses, particularly in treatments involving superficial brachytherapy. Muscles have a different density and atomic makeup when compared with other soft tissues. The distribution of radiation dose in the surrounding tissues can be impacted by variations in muscle density.

Tumor heterogeneities also arise during brachytherapy and the differences in tissue types and densities may exist inside the tumor. Treatment planning must take these variations into account since it may impact the tumor's response to radiation.

2.2.2 APPROACHES TO TISSUE HETEROGENEITIES

Several methods have been developed to account for tissue variations in brachytherapy the use of Computed tomography (CT) imaging is a popular technique that can be used to produce more precise dosage calculations by providing information about tissue densities. With the use of CT-based treatment planning tools, distinct densities can be assigned to various tissues, resulting in a more accurate depiction of the patient's anatomy according to Landry et al. (2016).

Monte Carlo simulations are another method utilized to handle tissue heterogeneities. The transportation of radiation particles through the patient's tissues is simulated using Monte

Carlo methods, which consider the interactions with various tissue types. Compared to conventional techniques, Monte Carlo simulations are more precise in accounting for tissue heterogeneities and can yield detailed information about the radiation dose distribution (Bauer et al.,2014).

Additional strategies are used to account for tissue heterogeneities. Utilizing strategies including intraoperative planning, real-time treatment adjustments, and pre-implant dosimetry, the dose administration is optimized according to the patient's unique anatomy and tissue heterogeneities.

2.2.3. CHALLENGES OF TISSUE HETEROGENEITIES

Precisely predicting the radiation dosage distribution throughout the heterogeneous tissues is a major challenge in brachytherapy. The homogeneity of the tissues assumed by conventional treatment planning techniques might result in large dosimetry inaccuracies. Tissue heterogeneities can alter the route, scattering, and absorption of the radiation beam, changing the dose that is administered. Consequently, increasing treatment accuracy requires sophisticated treatment planning algorithms that take tissue heterogeneities into account as emphasized by Peppa et al. (2016)

2.2.4. CHARACTERISTICS OF TISSUE HETEROGENEITIES

In brachytherapy, tissue heterogeneities encompass a range of characteristics that significantly influence radiation dose distribution and treatment outcomes. One key factor is density variations, which refer to differences in mass densities among various tissues. For instance, bone possesses a higher density compared to softer tissues such as muscle or fat. These variations in density can affect how radiation interacts with tissues, leading to changes in scattering patterns and dose deposition (Adelnia and Fatehi, 2016).

Another essential characteristic impacting radiation dose distribution is anatomic composition. The anatomic compositions of different tissues vary, which affects interactions with radiation. Tissues with lower atomic numbers, like muscle and fat, behave differently in response to radiation compared to those with higher atomic numbers, such as bone. Changes in anatomic composition can therefore influence how radiation is absorbed, scattered, and attenuated within tissues (Paganetti, 2015). Tissue heterogeneities within the patient's anatomy may have different spatial distributions. For instance, the tumor could be adjacent to bones, or soft tissues might encircle air spaces. Variations in the placement and configuration of tissue heterogeneities affect the radiation beam's path, resulting in different dosage distributions and deposition.

The size and shape of tissue heterogeneities might also differ and when compared to lesser heterogeneities, large heterogeneities, like an air cavity or a bone structure, might have a more noticeable effect on the radiation dose distribution. The scattering and shadowing effects on the radiation beam can also be influenced by the form of tissue heterogeneities.

Tissue heterogeneities frequently create boundaries or interfaces where the characteristics of the tissues suddenly change for one another. These interactions may result in dose perturbations, enhancements, or scattering effects that alter the radiation dose distribution.

Tissue heterogeneities may occasionally change over time. For example, a patient's anatomy may alter as a result of physiological conditions, or a tumor may shrink or disappear during treatment. To guarantee precise dosage distribution, these temporal variations in tissue heterogeneities necessitate close observation and treatment plan adaption according to Molinari et al. (2018).

2.2.5. IMPACTS OF TISSUE HETEROGENEITIES ON DOSE DISTRIBUTION

One significant effect of tissue heterogeneity on dose distribution in brachytherapy is dose perturbation caused by variations in tissue properties. Changes in tissue density and atomic composition can lead to differences in radiation absorption, scattering, and attenuation. As a result, certain areas of the target volume and adjacent healthy tissues may either receive too much or too little radiation. This imbalance can reduce tumor control or increase the risk of complications in nearby healthy tissues, adversely affecting the treatment's efficacy (Morcos et al., 2021).

The ability to achieve appropriate dose coverage in the target volume may be compromised by tissue heterogeneities. Variations in tissue densities around the target can cause radiation beams to deviate from the planned dose distribution. Inaccurate target coverage may jeopardize the treatment's effectiveness in completely eradicating tumor cells.

Additionally, tissue heterogeneities can affect the protection of surrounding organs at risk (OAR) from high radiation doses. The amount of radiation that reaches OAR can vary based on the densities and compositions of the surrounding tissues, potentially increasing the risk of complications or adverse effects. Therefore, it is essential to optimize treatment regimens through accurate identification of tissue heterogeneities to minimize radiation exposure to critical structures (Barry et al., 2021).

To address the impacts of tissue heterogeneities, advanced treatment planning approaches are required. It is crucial to effectively predict and quantify dose distribution in the presence of these variations, which entails optimizing the treatment strategy by integrating data on tissue densities, interfaces, and spatial relationships.

Tissue heterogeneities may also complicate treatment delivery. Variations in tissue densities can affect the precision of treatment delivery devices, such as external beam collimators or brachytherapy applicators. Therefore, adjustments may be necessary during treatment to ensure the correct positioning of radiation sources or to account for changes in tissue heterogeneities that may occur over time (Satpathy et al., 2019).

Lastly, tissue heterogeneities can influence variability in patient treatment outcomes. Different responses to radiation can arise from variations in tissue densities and compositions, which may affect tumor control rates and the incidence of adverse effects. Accurate assessment and characterization of tissue heterogeneity can help reduce variability and improve treatment outcomes (Wei et al., 2021).

2.2.6. STRATEGIES TO MITIGATE THE EFFECT OF TISSUE HETEROGENEITIES

Using a variety of techniques to account for tissue heterogeneities is essential for enhancing treatment delivery and planning in radiation therapy. Advanced treatment planning algorithms, such as pencil beam algorithms with heterogeneity correction and Monte Carlo techniques, are employed to more accurately consider tissue variances. These algorithms help minimize the effects of heterogeneities on treatment planning by factoring in different tissue densities and compositions during dose distribution calculations (Hueso-González et al., 2015).

Strict quality assurance procedures are essential to ensure the accuracy of treatment preparation and delivery, particularly when dealing with tissue heterogeneities. Regular calibrations and measurements are conducted to validate the precision of dose calculation algorithms, imaging systems, and treatment delivery systems, ensuring that the intended

dose is administered to the target volume while reducing the impact of heterogeneities (Esteva-Socias et al., 2019)

2.3. DOSE CALCULATION ALGORITHMS IN BRACHYTHERAPY

Calculating the radiation dose administered to the patient's tissues, dose calculation algorithms are essential to the planning of radiation therapy treatments. Based on the treatment settings and the anatomy of the patient, these algorithms anticipate the dosage distribution using mathematical models and computer methodologies (Chen et al.,2018).

Analytical algorithms are one of the commonly used dose calculation algorithms that is used to estimate the radiation dose which rely on analytical solutions and mathematical equations. According to Shajid et al. (2024), The TG-43 formalism is one of the widely used analytical approaches that is specifically intended for brachytherapy dosage estimations. It offers a streamlined method of determining dosage around a single radioactive source by taking into account variables including tissue attenuation, source strength, and shape. (Enger et al.,2020)

Deterministic algorithms, sometimes referred to as pencil beam algorithms, mimic how radiation beams behave as it passes through a patient's anatomy using mathematical computations. These techniques compute the dosage contribution from each voxel, which are tiny volume elements or voxels that make up the patient's anatomy. The Analytical Anisotropic method (AAA) and the Collapsed Cone Convolution Superposition (CCCS) method are two instances of deterministic algorithms (Fan et al.,2018)

Monte Carlo simulations are regarded as the gold standard for dose calculations due to its great precision. To replicate the movement of individual radiation particles through the

patient's tissues, it employs statistical techniques. To produce precise and comprehensive dose projections, Monte Carlo simulations take into account a variety of variables, including scattering, tissue heterogeneities, and radiation interactions. Nevertheless, Monte Carlo simulations might require a lot of time and be computationally intensive (Fan et al.,2018).

The benefits of Monte Carlo simulations and analytical methods are combined in model-based convolution algorithms. To pre-calculate dosage kernels or point spread functions (PSFs) that characterize the dose spread from a single radiation source or beam, they employ mathematical models. The dose distribution is then computed by convolving these kernels, or PSFs, with the patient's anatomy. Dose kernel or PSF model quality and complexity affect the accuracy of model-based convolution methods as stated by Neph et al. (2019).

The goal of hybrid algorithms is to increase efficiency and accuracy by combining the best features of several dosage calculation techniques. In various anatomical locations of the patient, these algorithms may combine the use of deterministic algorithms, analytical algorithms, or Monte Carlo simulations. Hybrid techniques leverage the capabilities of each algorithm to minimize processing time and produce accurate dose estimations as justified by Montero et al. (2017)

2.3.1. HOMOGENEOUS TISSUE ASSUMPTIONS

A typical simplification in radiation therapy treatment planning and dose calculations is the homogenous tissue assumption. It is predicated on the idea that a certain area or volume of tissue being treated has consistent atomic composition and density throughout.

One of the main tenets of the homogenous tissue assumptions according to Bocan et al. (2018) is that the homogeneous tissue assumption assumes that the tissue under treatment has a homogenous density. In actuality, adipose tissue distribution, the existence of bones, and air cavities cause differences in tissue density. The treated volume's density variations are disregarded by the homogenous tissue assumption.

Homogeneous atomic composition is one of the homogeneous tissue assumptions which indicates that the tissue undergoing treatment has a consistent atomic composition. The atomic compositions of various tissues vary, which might have an impact on how radiation interacts with the tissue. These differences in atomic composition inside the treated compartment are disregarded by the homogenous tissue assumption (Bocan et al.,2018)

An electron density approximation, in which the tissue is described by its electron density rather than its physical density or atomic composition, is occasionally used in conjunction with the homogeneous tissue assumption. By assuming that the electron density is the main component influencing radiation dose deposition, this approximation makes the computation of radiation interactions simpler (Zuo et al.,2018).

2.4. MONTE CARLO SIMULATION

Park et al. (2018) highlighted that Monte Carlo simulation is a highly effective computational technique widely utilized in radiation therapy for modeling and analyzing dose distribution. This stochastic method effectively predicts the behaviour of radiation particles as they interact with matter, enabling precise estimates of dose deposition within patient anatomy.

The focus of the research was to evaluate the dosimetry accuracy of the Gamma Med HDR brachytherapy treatment planning system, particularly in the context of tissue heterogeneities. The authors employed both experimental measurements and Monte Carlo simulations to assess dose distributions in heterogeneous phantoms. Findings revealed significant discrepancies between the planned and measured doses, underscoring the necessity of accounting for tissue heterogeneities in treatment planning.

Lesperance et al. (2014) investigated the impact of tissue heterogeneity on dosimetry in eye plaque brachytherapy. By utilizing Monte Carlo simulations and phantom experiments, Lesperance's study illustrated how ocular tissue heterogeneities influence dose distribution around the plaque, emphasizing the importance of patient-specific modelling for optimal treatment planning and delivery.

In another study, Taylor et al. (2016) demonstrated how tissue heterogeneity affects dosimetry parameters in high-dose-rate brachytherapy across various anatomical sites. Through Monte Carlo simulations and clinical case studies, Taylor's research illuminated the intricate relationship between tissue heterogeneities and dose distribution, highlighting the critical need for personalized treatment planning to accommodate patient-specific anatomical variations.

Fogliata et al. (2018) examined the effects of breast tissue composition such as glandular density and the fibro-glandular ratio on dose distribution within the target volume and surrounding healthy tissues. Fogliata's work underscored the importance of tailored treatment planning to optimize dose delivery and minimize toxicities in breast brachytherapy.

2.4.1. PRINCIPLES OF MONTE CARLO SIMULATION

Monte Carlo simulation involves repeatedly sampling random variables to obtain numerical results. In the context of radiation therapy, it simulates the transport of individual photons, electrons, or other particles through patient tissues.

The process tracks each particle's interactions, including scattering, absorption, and the production of secondary particles, as they move through the medium. By statistically sampling these interactions, the simulation creates a comprehensive picture of dose deposition throughout the target volume and the surrounding tissues (Paro et al., 2016)

2.4.2 ACCURACY AND VERSATILITY OF MONTE CARLO SIMULATION

Monte Carlo simulation is highly regarded for its exceptional accuracy in dose calculation. Unlike analytical algorithms, which frequently rely on simplifications and approximations, Monte Carlo methods offer precise modelling of intricate radiation interactions. This technique is adaptable and can be utilized across various treatment modalities, including external beam radiotherapy (EBRT), brachytherapy, and radiopharmaceutical therapy. It accommodates diverse radiation sources, energy spectra, and patient geometries with great ease.

2.4.3. APPLICATION OF MONTE CARLO SIMULATION IN TREATMENT PLANNING

Monte Carlo simulation is essential in treatment planning, where accurate dose prediction is critical. It provides a precise assessment of dose distribution both within target volumes and around critical organs, enabling clinicians to refine treatment plans that maximize tumor control while minimizing toxicity to healthy tissues, as highlighted by Moreno-Barbosa et al. (2020).

Moreno-Barbosa et al. (2020) noted that Monte Carlo simulations are particularly valuable in brachytherapy for modelling dose distribution around radioactive sources implanted in or near the tumor site. This capability allows clinicians to tailor treatment plans according to the specific anatomy of each patient and the positioning of the sources.

2.4.4. CHALLENGES AND CONSIDERATIONS OF MONTE CARLO SIMULATION

Despite its accuracy and versatility, Monte Carlo simulation can be computationally intensive and time-consuming, particularly for complex treatment scenarios and high-resolution simulations. Efficient implementation strategies and parallel computing techniques help mitigate these challenges (Knoll et al.,2022)

Validation of Monte Carlo simulations against measured data is essential to ensure their reliability and clinical relevance. This involves comparing simulated dose distributions with measurements obtained from phantoms or patient-specific dosimeters to verify accuracy and consistency according to Knoll et al. (2022).

2.5. REVIEW OF EMPIRICAL STUDIES ON TISSUE HETEROGENEITIES

Research on tissue heterogeneities in radiation therapy has yielded important insights into how differences in tissue affect treatment outcomes, dose distribution, and planning. These investigations frequently make use of dosimetry measures, imaging methods, and patient data to evaluate the impact of tissue heterogeneities.

One of the investigations according to Enger et al. (2019) on the review of empirical studies on tissue heterogeneities has assessed the precision and constraints of dose calculation algorithms when tissue heterogeneities are present. The accuracy of Monte Carlo

simulations, deterministic algorithms, and analytical algorithms in diverse scenarios has been compared in these works. Studies have emphasized how crucial it is to precisely represent tissue heterogeneities to enhance treatment planning and dosage estimations by Chopra et al. (2018).

Empirical studies have investigated the dosimetry effects of tissue heterogeneities on treatment planning, have examined the impact on target coverage, organ-at-risk sparing, and dose distribution in different treatment sites (Crowe et al., 2013). These studies have emphasized the need for accurate characterization and consideration of tissue heterogeneities to ensure optimal treatment plans (Huang et al.,2019).

Some empirical studies have explored the relationship between tissue heterogeneities and clinical outcomes in radiation therapy. Studies have investigated the influence of tissue variations on treatment response, tumour control rates, and complications. These studies have provided evidence of the importance of accounting for tissue heterogeneities to improve treatment outcomes and minimize the risk of complications (Crowe et al., 2013).

Empirical studies have evaluated the use of advanced imaging techniques, such as positron emission tomography (PET) and magnetic resonance imaging (MRI), in characterizing tissue heterogeneities. These studies have assessed the potential of incorporating functional and metabolic information from these imaging modalities to enhance treatment planning and target delineation (Huang et al.,2019)

Some empirical studies have focused on patient-specific approaches to account for tissue heterogeneities. These studies have investigated the use of personalized imaging data, such as dual-energy CT or MRI, to derive patient-specific tissue density maps for improved dose

calculations. They have highlighted the potential benefits of individualized approaches in treatment planning (Akhavanallaf et al.,2021).

2.5.1. EXPERIMENTAL METHODOLOGIES AND SETUPS OF EMPIRICAL STUDIES ON TISSUE HETEROGENEITIES

A variety of techniques and configurations are frequently used in experimental investigations which examine tissue heterogeneities in radiation therapy to evaluate the impact of tissue differences on dose distribution and treatment outcomes. These investigations often use common experimental sets and procedures.

In this research, real phantoms that replicate human tissues and anatomical structures are used. To mimic the characteristics of human tissues, these phantoms can be constructed from a variety of materials, including tissue- or water-equivalent polymers. Inserts or layers of various materials with differing densities or atomic compositions can be used to introduce tissue heterogeneities into the phantom. When tissue heterogeneities are present, radiation measures like ionization chamber or film dosimetry are carried out to assess the dose distribution (Katsarou et al.,2019)

To examine the impact of tissue heterogeneities, animal models such as mice, rats, or bigger animals are used in animal studies. Animal models can shed light on how the body reacts to radiation and how different tissues affect how well a therapy works. Tissue heterogeneities can be created artificially by implanting materials with varying compositions or densities, or they can occur spontaneously in animal models. To assess the dosage distribution and biological effects, imaging investigations, histological analysis, and dose measurements are frequently carried according to Vrbik et al. (2019)

Empirical research also uses patient data to assess the impact of tissue heterogeneities. This includes retrospective reviews of radiation therapy patients' clinical outcomes, imaging data, and treatment plans. Researchers can investigate the effects of tissue changes on dose distribution and treatment outcomes by comparing different patient cohorts or by establishing a link between dosimetry parameters and clinical outcomes. (Vrbik et al., 2029

Advanced imaging techniques such as computed tomography (CT), magnetic resonance imaging (MRI), or positron emission tomography (PET) are commonly used in empirical research to characterize tissue heterogeneities. These imaging methods provide information on tissue densities, anatomical features, and functional traits. Tissue density maps customized for each patient or an assessment of the effects of various tissues may be made using imaging data.

Dosimetry measurements are crucial in experimental studies of tissue heterogeneities. A range of dosimeters, such as ionization chambers, diode detectors, radio chromic films, and gel dosimeters, can be used to measure the radiation dosage when tissue heterogeneities are present. These measures give quantitative data on dose distribution, dose perturbations, and the accuracy of dose calculation techniques. Hasani and associates (2019) Experimental investigations may assess how well treatment planning systems (TPS) accommodate tissue heterogeneities, as claimed by Hasani et al. (2019). This entails evaluating the precision of dose projections against experimental measurements or reference data, or comparing dose computations made by various TPS algorithms.

CHAPTER THREE

MATERIALS AND METHODOLOGY

3.1 OVERVIEW

This chapter consists of all the materials and methods used to acquire the data of the research. It provides clear explanations of the methods, tools, and data gathering strategies used for this research work. Additionally, it provides detailed information of the site used and provides a summary of the statistical data analysis approach used in this investigation.

3.2. MATERIALS

The materials used in this study are the CIRS electron density phantom (EDP), Philips Computed Tomography (CT) scanner (US, 2016), High Dose Rate (HDR) Afterloader (Germany, 2013), PTW Unidos electrometer (Germany, 1997), Iba ionization chamber (Germany, 2023), Sodium hydroxide (NaOH), Total quartz engine oil (SAE 40), Frytol cooking oil, Radiant DICOM image viewer and check source.

3.2.1 THE ELECTRON DENSITY PHANTOM

The CIRS Electron Density Phantom (Figure 3.1) is a tool that is specifically designed and use in radiotherapy to establish the correlation between CT data and the electron density (ED)/physical density (PD) of various tissues in human body. The phantom consists of two nested disks that can be used to configure both head and abdomen. There are 17 slots in the scan field where nine distinct tissue equivalent electron density plugs can be placed and a vial plug that can be filled with any liquids. The accuracy of the CT scanner's distance measurement can be quickly evaluated with optional distance marker plugs. The electron density phantom is a preferred tool for medical physicist because it consists of features that

help to evaluate CT scan data, correct for inhomogeneities, document relationship between CT number and tissue electron density, simulate indicated tissue within the diagnostic energy range and quickly assess distance registration.

During routine quality assurance test, a medical physicist inserts the CIRS Electron Density Phantom into a CT scanner to ensure that, the CT scanner is measuring electron densities correctly. The scan results are compared to the materials of the phantom, which have known electron densities. The phantom is used to ensure that, newly installed imaging equipment can accurately interpret electron densities. This procedure, when follows will help to ensure that the equipment is correctly calibrated before using it for treatment planning and patient imaging.

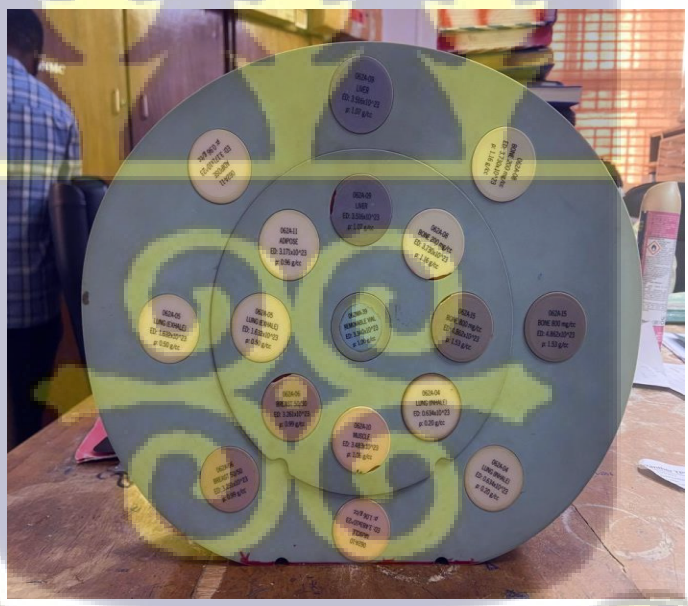

Figure 3. 1: Image of the CIRS electron density phantom at NRONMC

3.2.2 FABRICATED PHANTOM

In this research work, a square phantom represented in figure 3.2 with compartments, were designed using a Perspex sheets of thickness 3mm. The center of the phantom has a source

holder and a movable detector holder. The various compartments are concentric and designed in such a way that when the detector holder slide, it will still be or located within a compartment. The distance from the source at the middle of the phantom to the first compartment is 2.5 cm, 7.7 cm to the second compartment and 12.6 cm to the third compartment. Each chamber has an outlet at the base of the phantom for discharge of the materials. The phantom has the following measurements or dimensions as follows; height of phantom was 25 cm with the volume of the Phantom base as 30.6 cm x 30.6 cm x 30.6 cm. The compartment dimensions were given as 10 cm x 25 cm and 9.4 cm x 25 cm for compartment 1, 20 cm x 25 cm and 19.4 cm x 25 cm for compartment 2 and 30 cm x 25 cm and 29.4 cm x 25 cm for compartment 3. Additional two slots on the holder are tilted or varied to change the location of the measurement

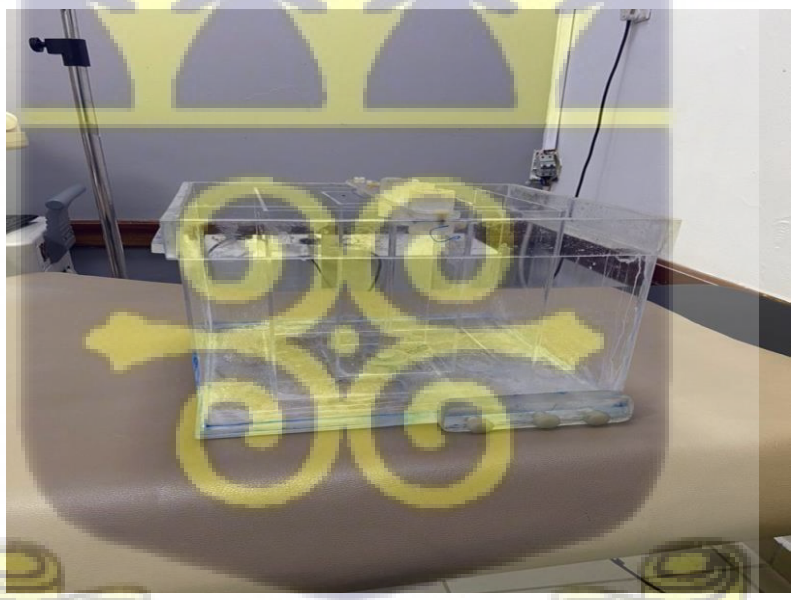

Figure 3. 2.: Image of the constructed water Phantom at NRONMC

3.2.3 THE PHILIPS COMPUTED TOMOGRAPHY (CT) SCANNER

The scanning of the ED phantom and the selected materials was conducted at the Radiology Department of the University of Ghana Medical Center (UGMC) using a Philips Medical Systems CT scanner, as shown in Figure 3.3. The scanner model is MRC 880, with a serial number of 32170, and it features 64 slices. Its kilovoltage peak ranges from 80 to 140, with automatic mAs selection.

This CT scanner employs advanced computer-processing technology to generate cross-sectional images, commonly referred to as slices, of specific areas of interest, such as bones, blood vessels, and soft tissues. By combining numerous X-rays and measurements taken from various angles, the system creates detailed and accurate images. Compared to standard X-rays, CT scans provide significantly clearer and higher-resolution images, as a result of the scanner's sophisticated design and capabilities.

Figure 3. 3: the Philips computed tomography (CT) scanner at the UGMC facility.

3.2.4 HIGH DOSE RATE (HDR) AFTERLOADER

The National Radiotherapy, Oncology, and Nuclear Medicine Center (NRONMC) at Korle Bu Teaching Hospital in Accra, Ghana, utilizes an HDR Afterloader brachytherapy system with a Cobalt-60 (Co-60) source, as shown in Figure 3.4. This Multisource HDR Afterloader system, manufactured by Eckert & Ziegler, supports up to 40 channels with advanced channel coding, ensuring optimal safety even for the most complex implants.

The HDR brachytherapy Afterloader is designed to conserve space efficiently and includes an integrated in-vivo dosimetry system for enhanced functionality. The device is user-friendly and comfortable to operate. HDR brachytherapy procedures can be performed with a range of applicators, templates, needles, and catheters, offering flexibility for different clinical needs

Figure 3. 4: image of the high dose rate (HDR) Afterloader at NRONMC, 2024

3.2.5 C-ARM MOBILE X-RAY MACHINE

One piece of technology that makes brachytherapy sessions run smoothly and quickly is the Flourostar Mobile Digital C-Arm as shown in Figure 3.5 below. Its preview collimation feature, which allows users to preview shutter/iris collimator positioning without exposure, contributes to a reduction in the overall dose to patients and staff.

The technology makes it simple for users to choose a pre-defined fluoro mode for imaging the anatomy at the best mA and kV values, thus reducing dosage even further. Additionally, it has improved post-processing capabilities with a dual-side touchscreen interface that provides the user with instant access to all post-processing features, making photography quick and easy.

The C-arm mobile X-ray machine is used in the field of diagnostic radiology and interventional radiology. It is primarily employed for real-time imaging during surgical, orthopedic, and interventional procedures, allowing clinicians to view internal structures and guide instruments accurately during operations

Figure 3. 5: C-arm mobile x-ray machine at NRONMC, 2024

3.2.6 THE PTW UNIDOS ELECTROMETER

The PTW UNIDOS Electrometer showed in figure 3.6 is a vital tool for medical physicist working in radiation therapy. It was made by Freiburg in Germany and it primarily used to measure dose, dose rate, charge and current and displays its results in various units Gray (Gy), Sievert (Sv), Roentgen (R), etc.

The UNIDOS Electrometer is unique because of its easy-to-use design and also compactible with ionization chambers and solid-state detectors and can also be used for a wide range of radiation measurements, including those involving photons, electrons, and protons, due to its great versatility and compatibility with various ionization chambers and

detectors. Furthermore, it allows for air density corrections base on air pressure and temperature or through a radioactive check device.

In addition to its technological features, the PTW UNIDOS Electrometer is also important for patient care. It ensures that, patients receive the appropriate radiation dose, which is essential for the efficacy and security of therapy, by offering precise dosimetry measurements. Measurement data may be stored, transferred, and analyzed more easily because of its strong data management features, and also provide comprehensive documentation and quality control. The UNIDOS Electrometer is a vital instrument for clinics committed to giving their patients the finest care possible because, it essentially makes a significant contribution to the overall safety and efficacy of radiation therapy.

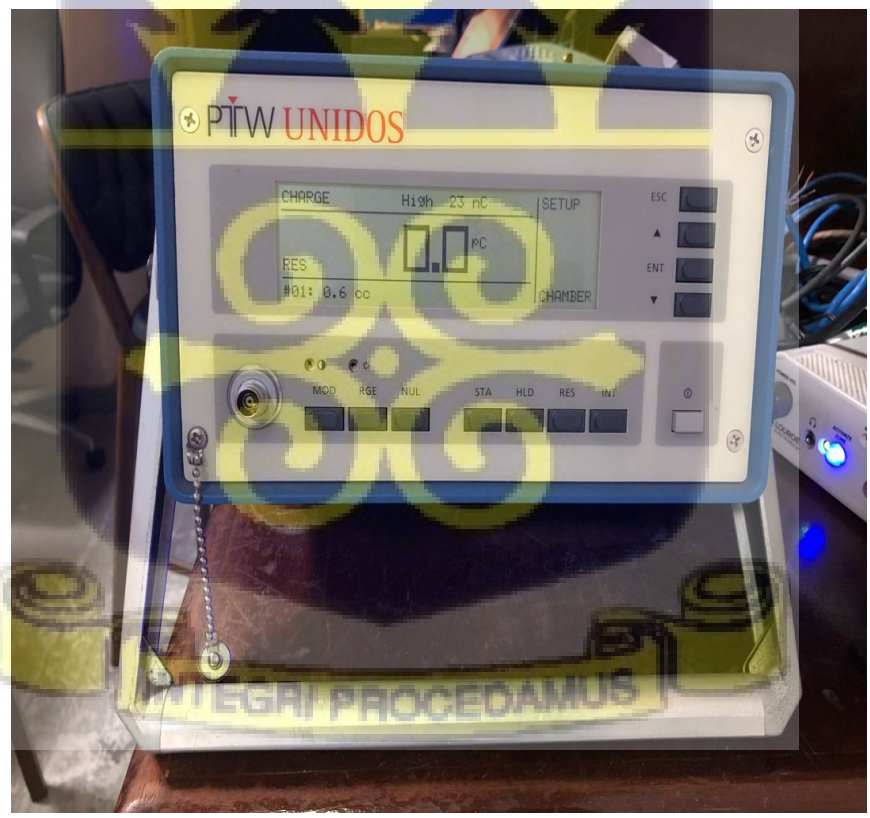

Figure 3. 6: the PTW UNIDOS electrometer at NRONMC

3.2.7 IBA IONIZATION CHAMBER

The IBA (Ion Beam Applications) ionization chambers as shown in Figure 3.7 below are highly accurate radiation dose meters that are used extensively in radiation therapy for dosimetry and quality control. It is widely recognized for accuracy in measuring doses, which guarantees that radiation therapy is administered precisely. The chamber provides a constant and consistent reaction over an extended period of time, that is acceptable for repeated assessments and continuous use.

To ensure traceability and reliability in the dosimetry readings, the chambers are typically calibrated in accordance with national standards. Certain IBA ionization chambers have narrow sensitivity that enables accurate measurements in narrow radiation fields, which is key for high-precision procedures like stereotactic radiosurgery.

These chambers are excellent for a wide range of radiation types and energies since it frequently has minimal energy dependence, easy connection interfaces and clear labels based on design. The IBA ionization chambers that are used for water phantom measurements can be employ to verify doses under conditions that are comparable to those in water. The IBA ionization chambers can be used in a variety of clinical and research settings since it is frequently interoperable with different electrometers and dosimetry systems.

Figure 3. 7: Image of the IBA ionization chamber with its buildup cap on and in its protective case at NRONMC

3.2.8 SODIUM HYDROXIDE (NaOH)

One of the three selected materials to simulate Liver tissue is Sodium Hydroxide (NaOH) as indicated in Figure 3.8 below. It is also known as caustic soda or lye which is highly caustic and alkaline chemical compound. Sodium Hydroxide are commonly used in many industries for soap making, paper manufacturing, and chemical production. Sodium Hydroxide is a white solid substance that easily dissolves in water to form a strong alkaline solution. The NaOH is corrosive and can cause severe burns to the skin and eye if not handled properly. It has a physical density of 1250 kg/m^3.

Figure 3. 8: A picture of a distilled water gallon containing Sodium Hydroxide (NAOH) solution at NRONMC, 2024

3.2.9 TOTAL QUARTZ ENGINE OIL (SAE 15-40)

The Total Quartz Engine Oil, SAE 15W-40 in Figure 3.9 is a high-quality, multi-grade engine oil that is made to work better in gasoline and diesel engines. The "15W-40" means that the oil has a viscosity rate of 15 in cold weather (W stands for winter) and 40 in hot weather. It provides good lubrication, which reduces wear and tear on engine parts and helps keep engines clean. It has a physical density of 868.4kg/m^3 at 15 ℃ and 872.5 kg/m^3 at 30℃ and may simulate an Adipose tissue.

Figure 3. 9: A gallon containing total quartz engine oil (SAE 15-40)

3.2.10 VEGETABLE (FRYTOL) OIL

The third tissue equivalent material selected is the Frytol cooking oil in Figure 3.10 below which is a popular brand of vegetable oil in West Africa, particularly in Ghana. It is usually made from a blend of vegetable oils, like sunflower, soybean, or palm oil. Frytol cooking oil can be used for baking, frying, and other cooking methods. It is often fortified with antioxidants to prevent oxidation and extend its shelf life. Its neutral taste and stable frying properties make it a popular choice in many homes and restaurants. It has a physical density of 900kg/m^3.

Figure 3. 10: Gallons containing of vegetable (Frytol) oil cooking oil.

3.3 EXPERIMENTAL PROCEDURE

The experimental procedure used in this research work to obtain the results for the discussion have been grouped in to four stages. The first step was the selection of Tissue Equivalent Materials, determination of the Hounsfield Unit (HU) units, Data collection and the processes of analyzing the data collected.

3.3.1 RESEARCH SITE

The study was conducted at the National Radiotherapy, Oncology, and Nuclear Medicine Center (NROMC) at Korle-Bu Teaching Hospital in Accra, Ghana. This Center of Excellence, located on Guggisberg Avenue, Korle-Bu, was chosen due to its proximity and

the availability of all necessary equipment for the study. Established in 1997, the center provides care to nearly 1,500 patients annually from across Ghana and the sub-region.

In addition to its clinical services, the NROMC serves as a research hub and is affiliated with professional bodies such as the Ghana College of Physicians and Surgeons, the Ghana College of Nursing and Midwifery, the Ghana College of Pharmacy, the School of Biomedical and Allied Health Sciences, and the University of Ghana.

The scanning of the electron density (ED) phantom and the selected materials was conducted at the University of Ghana Medical Center (UGMC) in Legon, Accra. The UGMC is a multidisciplinary tertiary healthcare facility known for its focus on achieving optimal clinical outcomes. It is equipped with state-of-the-art technology, making it one of the most modern medical centers in the region

3.3.2 CT QUALITY ASSURANCE (QA) TEST

Before the CT images of the known tissue equivalent materials and the selected equivalent materials were taken, a quality assurance (QA) test was done on the CT scanner to make sure the X-ray tube is ready for use and can minimize the risk of damage. At the University of Ghana Medical Center (UGMC), the quality assurance (QA) test is done daily and the required equipment for the test is the water-filled, cylindrical phantom which was provided by Philips, the manufacturer of the CT scanner at UGMC at the time of installation.

During the daily QA text procedures, the X-ray tube was allowed to warm up to an acceptable recommendation. Calibration scans (also called air-calibration scans) were performed to normalize the detector signals. The quality control (QC) phantom was placed

on the holder device at the isocenter of the scanner using the laser alignment lights of the scanner and also the alignment marks on the phantom surface.

A set up scan of the QC phantom was done using the scanner's daily QC scan parameter settings. During the process, the water mean and standard deviation values were monitored in both the axial or helical scan mode. An image was selected from the central portion of the phantom to analyze with a window width (WW) =100 and window level (WL) = 0. Five regions-of-interest (ROIs) were then drawn on the reconstructed image with area, approximately, 400 mm^2 at the center and other four spatial positions (12 o'clock, 3 o'clock, 6 o'clock, and 9 o'clock). The positions are related to specific locations on the circular reconstructed image.

The mean CT numbers for all five ROIs and the standard deviation of the center ROI were recorded on a datasheet. The uniformity value which includes the absolute value of center mean CT number and the peripheral mean CT number for the four edge ROIs. Finally, the images were carefully examined to check if artifacts such as rings or streaks are presents.

3.3.3 CALIBRATION OF THE ED PHANTOM AND THE SELECTED MATERIALS.

As illustrated in the setup shown in Figure 3.12, the Hounsfield units of the known tissue-equivalent materials were determined using an electron density phantom containing inserts with predefined electron densities corresponding to various tissue types. The phantom, with the tissue-equivalent materials inserted, was positioned on the CT scanner table. Appropriate scan parameters, such as tube voltage (kVp), slice thickness, and reconstruction algorithms, were configured to replicate the clinical settings typically used for patient scans.

The scans were performed separately for the known tissue-equivalent materials and the selected materials. Each material was scanned at tube voltages of 80, 100, 120, and 140 kVp, with the mAs values automatically adjusted based on the selected kVp. The kilovoltage peak (kVp) is the peak voltage along the X-ray tube in the CT scanner. It regulates the photon energy (or quality) produced by the X-rays. The effects of the kVp on the quality of the image is that, when the X-rays energy is higher, it can penetrate through the tissues more easily. It leads to the contrast between soft tissues been lessened, whiles improving the visibility of denser structures like the bones. Increasing the kVp, lowers the image noise and usually results in higher radiation dose to the patient.

Milliampere-Seconds (mAs) are the product of the tube current (measured in milliamperes, mA) and the exposure time (measured in seconds, s). It shows how many X-ray photons are created throughout the scan. Increased X-ray photons produced by higher mAs numbers can lead to an improved signal-to-noise ratio and also produce sharper or clearer images. This is particularly important in trying to visualize small details. The radiation exposure to the patient is directly increased with increasing mAs. Achieving a balance between patient safety and image quality, requires optimizing mAs. In obtaining the CT images of the known tissues inserted in the phantom already and the selected materials, ensuring that the scan covered the entire area of the phantom. The CT scanner reconstructs the images after scanning and the reconstructed images contains several gray levels with different Hounsfield units.

Figure 3. 11: A set-up of the ED phantom for CT scan during the study.

3.3.5 DETERMINATION OF HOUNSFIELD UNITS OF THE MATERIALS.

To determine the Hounsfield Units (HUs) from the reconstructed CT images, regions of interest (ROIs) corresponding to the tissue-equivalent and selected materials were identified and analyzed. The measurements were performed using the Radiant DICOM image viewer software, which calculated the HUs within each ROI. The HU value for each ROI was obtained as the average of the pixel intensities, with each pixel intensity directly corresponding to a specific HU.

For each kVp setting, three high-resolution slices with minimal artefacts were selected for analysis. The HUs were measured for each slice, and the recorded values were averaged to obtain the mean HU for each material.

3.3.6 DETERMINATION OF THE ELECTRON DENSITY AND THE RELATIVE ELECTRON DENSITIES OF THE MATERIALS.

To determine the electron densities (ED) and relative electron densities (rED) of the selected materials, the Hounsfield Units at each of the kVp's selected are grouped into positive and negative values. Both the positive and negative values were used to plot two separate graphs. The electron density (ED) values were plotted on the x-axis and the HU on the y-axis. Each of the graphs produces an equation along the y-axis and the regression (R^2). These equations were used to calculate the electron density (ED) of the selected materials at each kilovoltage.

Equation (1) is the equation generated by the graph of the positive values under 80 kVp. Equation (2) was also generated by the negative values of the graph under 80 kVp. The "x" Is the Hounsfield Unit (HU) of the electron density of the selected materials.

$y = 0.0012x + 3.3859$ eqn (1)

$y = 0.0034x + 3.391$ eqn (2)

Equations (3) and (4) were also generated from both the positive and the negative graphs respectively. The two equations were generated under a kilovoltage peak (kVp) of 100 and the "x" in both equations represent the Hounsfield Unit measured from the selected materials.

$y = 0.0014x + 3.4097$ eqn (3)

$y = 0.0034x + 3.387$ eqn (4)

The above equations, (5 and 6) were generated under the kilovoltage peak (kVp) of 120 plotted graphs. Equation (5) was generated from the positive values and also equation (6) was produced from the negative values from the 120 kVp and the "x" represents the Hounsfield unit (HU) of the of the selected tissue equivalent materials.

$y = 0.0017x + 3.3992$ eqn (5)

$y = 0.0033x + 3.3414$ eqn (6)

The two equations, (7) and (8) were generated from the 140 kVp graph plotted and they represent positive and negative values of the Hounsfield units of the known tissue equivalent materials respectively. The positive equation from the positive values has a regression (R^2) so as the negative values from the Hounsfield Unit (HU) of the known equivalent tissue materials.

$y = 0.0018x + 3.3984$ eqn (7)

$y = 0.0034x + 3.3684$ eqn (8)

The relative electron density (c) of both the known tissue equivalent materials and the selected tissue equivalent materials were calculated by finding the ratio of the electron density (ED) of the material and the electron density (ED) of water. This is expressed as;

$$\text{Relative electron density (rED)} = \frac{\text{Electron density of the material (ED)}}{\text{Electron density of water (EDW)}} \quad \text{eqn (9)}$$

3.3.7 QUALITY ASSURANCE OF BRACHYTHERAPY

The following quality assurance tests were performed at the brachytherapy department before the experiment to take the data began at the National Radiotherapy Oncology and Nuclear Medicine Center (NRONMC), the set up is first done as illustrated in Figure 3.12.

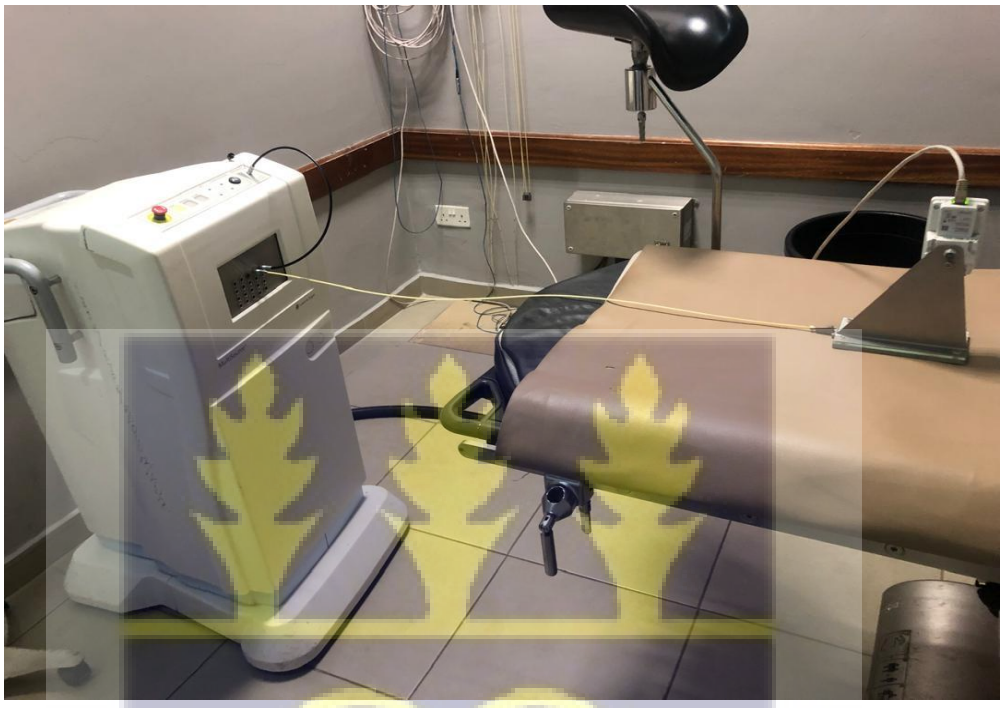

Figure 3. 12: A setup for the quality assurance performed during the study in 2

3.3.7.1 TIMER CHECK

As shown in Figure 3.14, before the experiment took place, a timer test was performed on an HDR after loader which is necessary for ensuring the accuracy and reliability of the timing system, which controls the duration at which the radioactive source spends at each dwell position. Accurate timing is important for delivering the prescribed radiation dose correctly. Two independent timers operate continuously in the system to monitor dwell times. For instance, if the time difference is greater than 1.5 seconds (> 1.5 sec.) at a dwell

point or greater than 3 seconds (> 3 sec.) for the total irradiation time in a channel, the treatment in progress is terminated. The test checks whether the system reacts properly to a time difference when it occurs. In performing the test, the timer check button was clicked, and then pressed the start button on the start-stop control panel. If the system is working properly and recognizes the difference, the corresponding message is displayed. Confirm the completed timer check with OK.

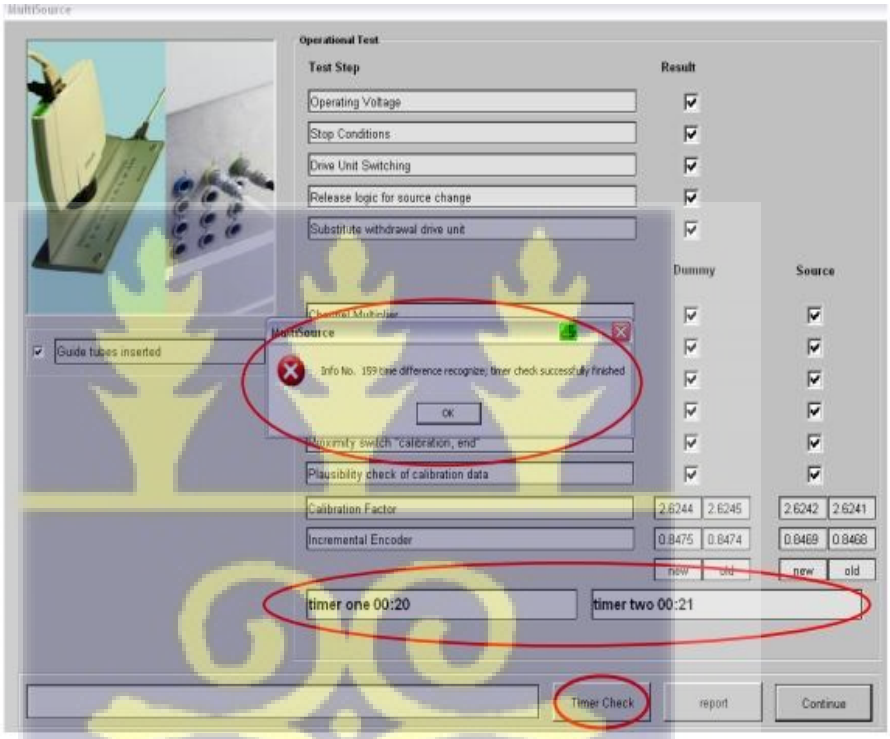

Figure 3. 13: An interface displayed on the TPS during the Timer Check procedure in 2024.

3.3.7.2 VISUAL TEST

As shown in Figure 3.14, performing a visual test was performed on the source drive mechanism in an HDR after loader which is very necessary for ensuring the proper functioning and safety of the system. The source drive mechanism is responsible for accurately moving the radioactive source to the correct positions during treatment. Before

a visual test was done, the Source Position Indicator (SPI) was connected through a guide tube to the required channel of the channel multiplier. During the connection of the Source ensuring that the guide tube is fully extended because when it bends, it negatively impacts the source positioning. The visual test function was then selected and before starting the visual test, a confirmation of the query that the Guide Tube is inserted into the channel by setting a check mark, and then pressing the start button on the start-stop control panel.

After the dummy, the source moves into the source position indicator. To check the precision of positioning, the source has to approach three dwell points within a tolerance range of ± 1 mm.

No correction is necessary as long as the source stops within the tolerance range. In contrast, if the source stops outside the tolerance range (e.g. at 7 mm for the 1st dwell point), a correction is necessary. In this case, the source position that is read off (e.g. 7 mm) is entered under the actual position and saved and the test procedure is repeated to check it; i.e. confirm the query repeat check by setting a check mark, and then press the start button on the start-stop control panel when requested to do so. Note if the source moves again to a position outside the tolerance range after correction, there is an error in the drive system. In this case, contact the Eckert & Ziegler BEBIG GmbH service department. The visual test was successfully completed when the source was moved to the three prescribed dwell points within the respective tolerance ranges.

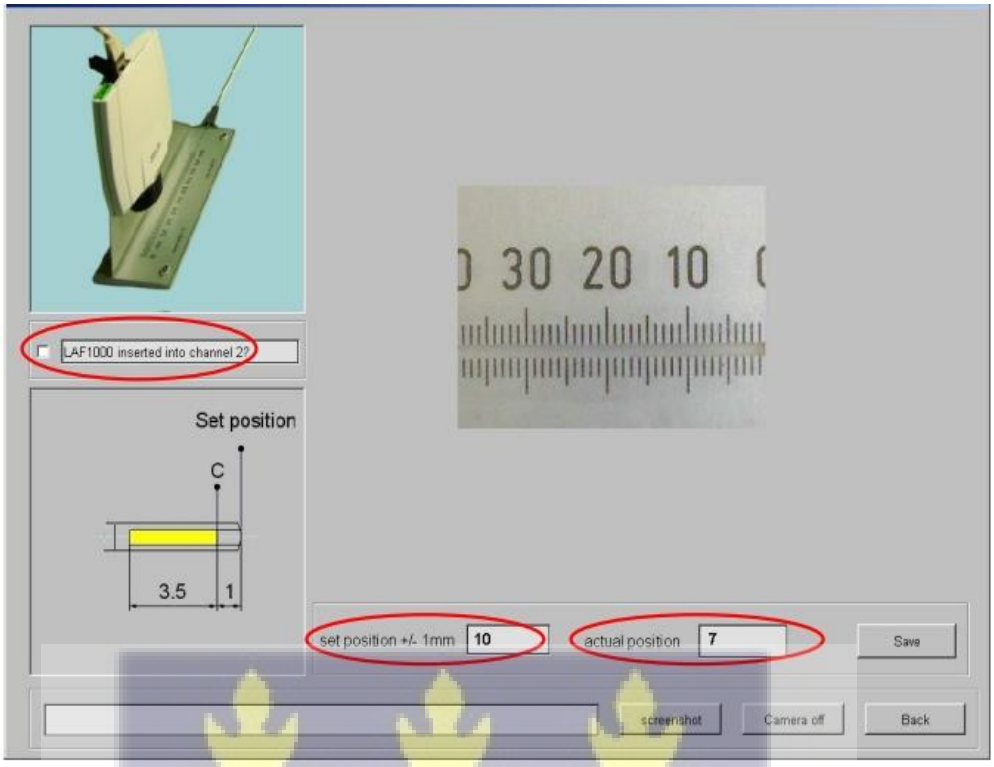

Figure 3. 14: An interface displayed on the TPS during the Visual Test procedure in 2024 at NRONMC.

3.3.7.3 CALIBRATING THE DUMMY AND THE SOURCE DRIVE

As shown in Figure 3.15, to calibrate the drive systems, the guide tube was connected to the Drive Check (DC) connection on the control panel and a required channel of the channel multiplier. The Calibration source/dummy function was selected to confirm the query guide tube inserted by setting a check mark. Next, the procedure was started. When the tests were completed successfully, it was confirmed automatically with a checkmark which was shown under the result. An error message will be displayed if the test fails. I started the calibration of the source drive after I had successfully completed the dummy drive test.

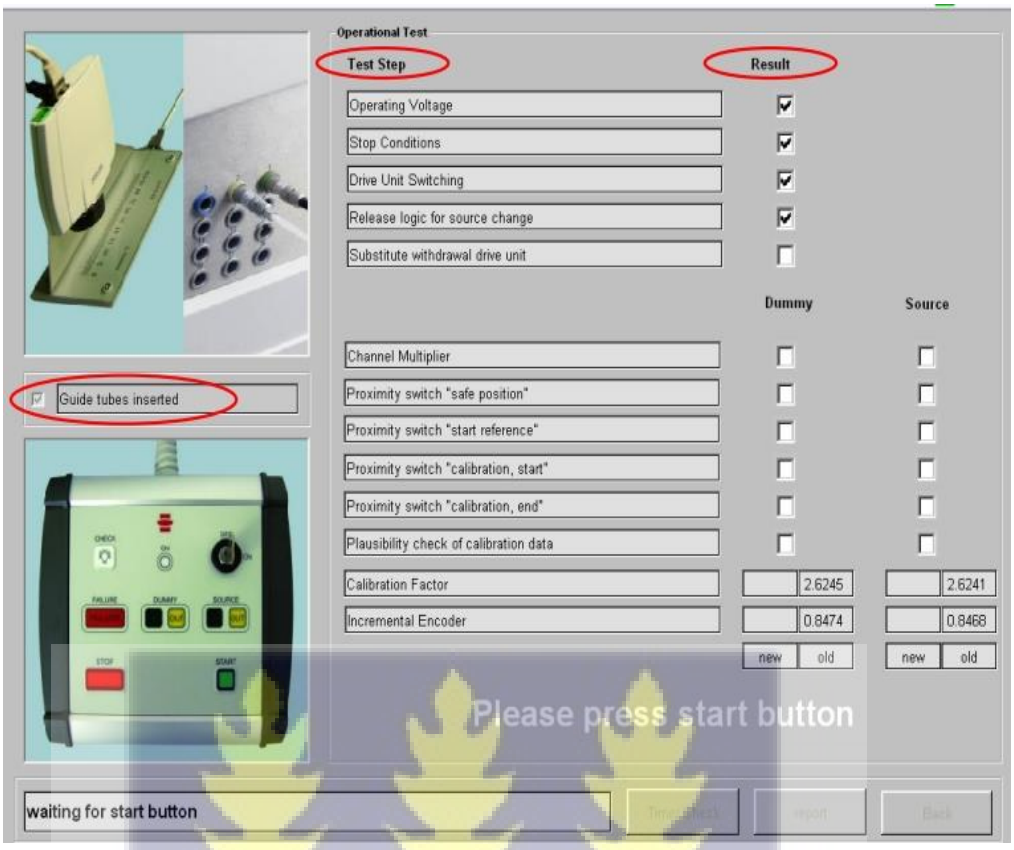

Figure 3. 15: interface displayed on the TPS during the calibration of the dummy and the source drive procedure in 2024 at NRONMC.

3.4. PHANTOM MEASUREMENT OF THE SELECTED MATERIALS

Two types of measurements were done during the measurement or irradiation of the selected materials and in each case, the fabricated phantom was used to replicate the human body. The homogeneous phantom measurement and the heterogeneous phantom measurement were done during this period. In the homogeneous phantom measurement, five different types of irradiations took place based on the materials selected. The measurement was done for air, water, sodium hydroxide (NaOH), total quartz engine oil (SAE15-40) and vegetable (Frytol) oil. Because is a homogeneous measurement, each of the chambers was filled with the same materials at a particular time. In all instances, the

initial temperature and pressure were taken before the measurement was done in each chamber and also, the final temperature and pressure were taken at the end of each chamber measurement.

During the heterogeneous phantom measurement, three materials (NaOH, SAE15-40 and Frytol cooking oil) were permutated into six groups and each was measured during the experiment. Each of the three chambers was filled with one of the three materials selected and before the measurement, the initial temperature and pressure were taken while the final temperature and pressure were taken after the measurement. Figure 3.16 is a set up during the phantom measurement of the materials.

Figure 3. 16: A set-up during the phantom measurement of the materials in 2024 at NRONMC

CHAPTER FOUR

RESULTS AND DISCUSSION

4.0 OVERVIEW

This chapter presents the results of the quality control tests done on the CT scanner before scanning the materials and the findings emanating from the research work done. The results and discussions outlined in this chapter include the findings from the determination of the relative electron densities (rED) and the Hounsfield Units (HU) of inserts provided with the commercial tissue characterization phantom (CIRS electron density calibration phantom) scanned using different kilovoltage peak of 80, 100, 120, and 140 kVp. It also consists of the findings of the electron densities (ED) and the relative electron densities (rED) of the selected materials, the findings of the measurements of all the materials during the homogeneous and heterogeneous measurements.

4.1 QUALITY CONTROL TEST

The data presented in Table 4.1 shows that the CT scanner used to scan the tissue characterization phantom passed the CT number uniformity test based on the recommendations of the International Electrotechnical Commission (IEC 61223-3-5 and IEC 61223-2-6). This result indicates that CT images acquired with the CT scanner would be devoid of artifacts and effects of beam hardening (Njiki et al., 2018). By analyzing the differences between the HU values at the central Region of Interest (ROI) and those at the peripheral positions (specifically at 12 o'clock, 3 o'clock, 6 o'clock, and 9 o'clock), it was found that all the measured differences were within the acceptable tolerance range, which is defined as 4 HU or less. This uniformity test was done using the water phantom provided by the manufacturer of the CT scanner (Sookpeng et al., 2016)

Using 0 HU as the baseline (water), all measured CT numbers across the four peripheral ROIs were within ±5 HU, confirming excellent image uniformity and scanner stability (Steiding et al., 2014).

Table 4. 1: CT Number (CT #) Uniformity Test Results

CT # UNIFORMITY	DIFFERENCES IN CT#	TOLERANCE ≤ 5HU
ROI 2 (12 O'clock)	-0.5697	PASS
ROI 3 (3 O'clock)	-1.2513	PASS
ROI 4 (6 O'clock)	-0.8723	PASS
ROI 5 (9 O'clock)	-0.3065	PASS

4.1.1 HIGH-CONTRAST RESOLUTION TEST

This was done to evaluate the accuracy of the CT scanner in differentiating various materials based on their density. According to Kim et al. (2019), the scanner measures the CT numbers (Hounsfield Units) of known materials (inserts) and compares them with expected values. The acceptance criteria typically depend on how closely the measured CT numbers match the expected ones. The small deviations observed were within the acceptable limits for clinical CT scanners. Based on the data set provided in Table 4.2, the contrast test results are acceptable, demonstrating that the CT scanner is functioning correctly and producing reliable measurements (Cropp et al., 2013).

Table 4. 2: Insert test results

Insert Material	Expected CT Number (HU)	Measured CT Number (HU)	Deviation (HU)
Air	-1000	-998	+2
Water	0	2	+2
Bone Equivalent	+1000	+995	-5

4.1.2 CT IMAGE NOISE

As detailed in Table 4.3, the CT image noise levels were below the 5 HU threshold. This outcome indicates the successful completion of the CT image noise test. The low noise levels demonstrate that the CT scanner's optimal performance in minimizing image noise contribute to the production of high-quality diagnostic images.

Table 4. 3: CT IMAGE NOISE RESULTS

NOISE (STANDARD DEVIATION)	TOLERANCE (5 ≤ HU)
3.993	PASS

4.2 RELATIVE ELECTRON DENSITIES AND HOUNSFIELD UNITS

The data presented in Table 4.4 reveals a pattern that categorizes the known tissue-simulating inserts within the electron density phantom into two distinct groups. According to the AAPM Task Group 43 (TG 43) report, water is used as the standard reference

medium. Tissues with relative electron densities greater than water (rED of water =1) are classified as denser materials, while those with densities less than the reference medium are considered less dense materials.

From Table 4.4 below, all tissues with densities greater than water showed positive Hounsfield Unit (HU) values across the selected kilovoltages (80, 100, 120, and 140 kVp). These include Muscle, Bone (800 g/cc), Bone (200 g/cc), and Liver. In contrast, tissues such as Lungs (exhale), Breast, Lungs (inhale), and Adipose, which have lower densities than standard reference medium (water), exhibited lower HU values. Table 4.4 also indicates that tissues with lower relative electron densities compared to water consistently show lower HU values when compared to tissues with higher densities.

Table 4. 4: Results of the determination of rED and HU of the known tissues inserted in the phantom

INSERTS	TISSUE	ED ($\times 10^{23}$)	rED	HU			
				80 kV	100 kV	120 kV	140 kV
062A-05	Lungs (exhale)	1.632	0.489	-498.474	-496.337	-495.423	-493.823
062A-06	Breast	3.261	0.976	-48.5	-33.807	-24.675	-27.483
062A-10	Muscle	3.483	1.043	53.191	42.835	43.317	39.323
062A-04	Lungs (inhale)	0.634	0.19	-831.625	-830.261	-831.67	-823.932
062A-15	Bone 800 g/cc	4.862	1.456	1252.418	1004.458	870.812	786.213
062A-08	Bone 200 g/cc	3.73	1.117	335.317	363.658	232.202	206.853
062A-09	Liver	3.156	1.053	62.208	51.333	51.073	48.668

062A-11	Adipose	3.17	0.949	-65.535	-70.483	-41.658	-60.433
062A-39	Water	3.34	1	5.56	-21.67	-18.88	-20.063

4.3. CORRELATION BETWEEN ELECTRON DENSITY AND HOUNSFIELD UNITS OF INSERTS WITHIN THE PHANTOM AFTER GROUPING.

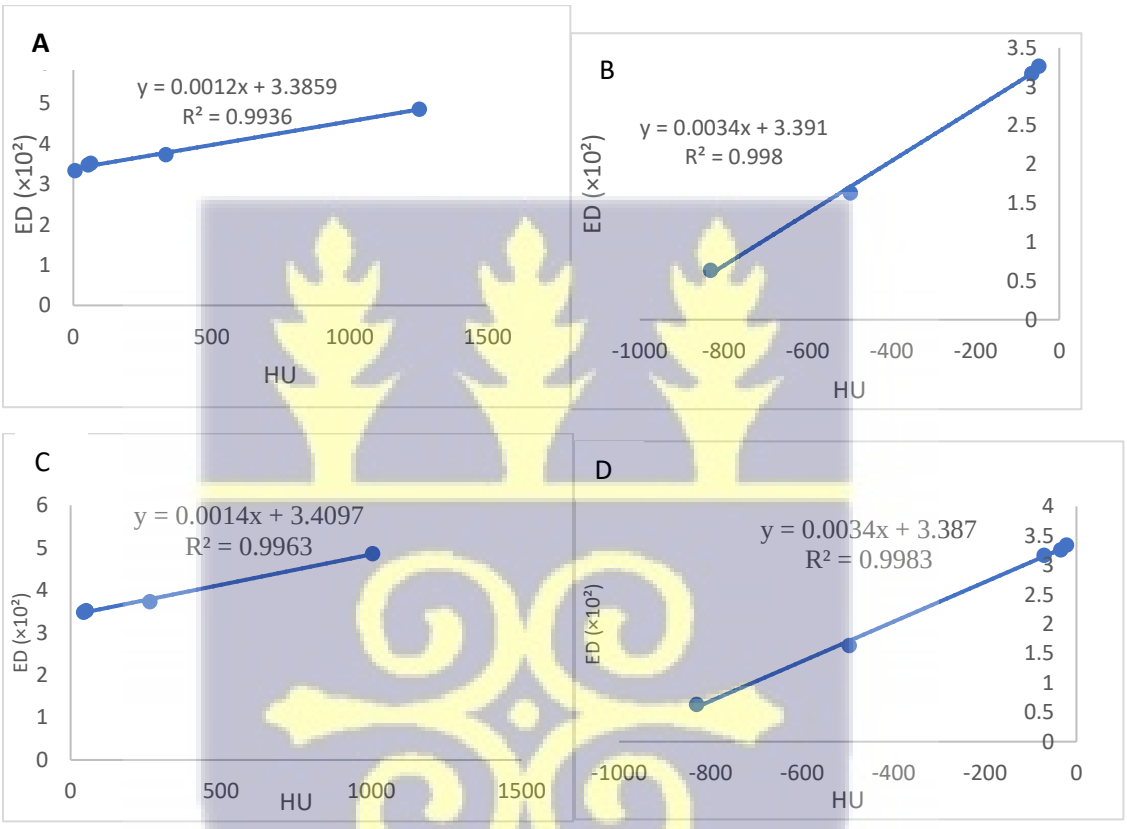

Figure 4. 1: Linear relationship between ED and HU scans. A) Positive HU at 80kV B) With negative HU at 80kV C) With positive HU at 100kV D) With negative HU at 100kV

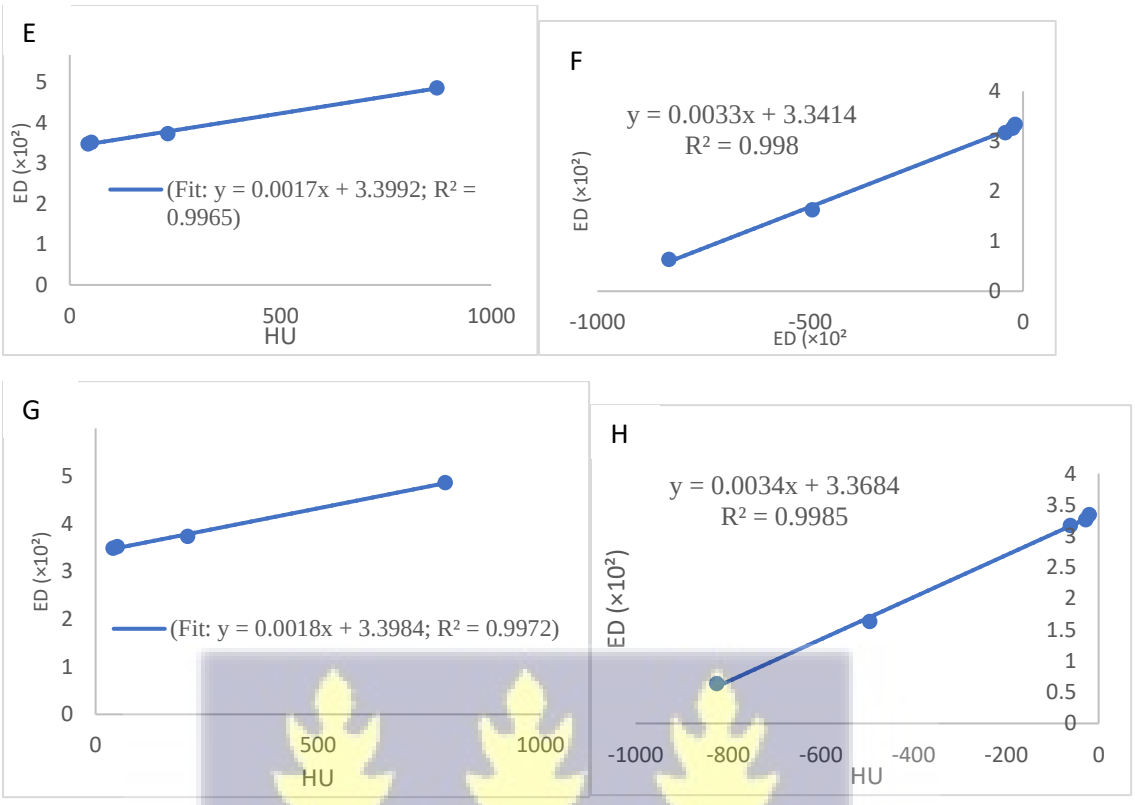

Figure 4. 2: Linear relationship between ED and HU scans. E) Positive HU at 120kV F) With negative HU at 120kV G) With positive HU at 140kV H) With negative HU at 140kV.

The graphs shown in Figures 4.1 and 4.2 illustrate the linear relationship between electron densities (ED) and Hounsfield Units (HU) derived from CT scans of tissues inserted in the electron density phantom. Figures A and B specifically display data obtained at 80 kVp. Figure A represents a graph generated using positive HU values, corresponding to tissues denser than water, while Figure B represents negative HU values for tissues less dense than water under the same 80 kVp conditions.

The regression coefficients (R^2) for Figures A and B, indicating the correlation between ED and HU, are 0.9936 and 0.998, respectively. The equations derived from the graphs were $y = 0.0012x+3.3859$ for Figure A and $y=0.0034x+3.391$ for Figure B.

Figures C and D also represent graphs generated under 100kV with Figure C being the positive values graph generated whereas Figure D was plotted using the negative values which are less dense when compared with the reference medium. The regression (R^2) that shows the correlation between the ED and HU are 0.9983 and 0.9983 for Figures C and D respectively. The generated equations for the two graphs are 0.0014x + 3.4097 and y = 0.0034x + 3.387 respectively. The graphs plotted under 120 kV are figures E and F. Figure E has a regression (R^2) of 0.9965 from the graph with positive values with an equation, y = 0.0017x + 3.3992 generated from the graph. Also, graph F was generated from the negative values which has a regression (R^2) of 0.90983 with its corresponding equation as y = 0.0033x + 3.3414.

Finally, graphs G and H were generated from the scans done at 140kV when the electron density (ED) plotted against the Hounsfield Units (HU) and it shows the linear relationship between them. The regression (R^2) between the positive and negative values for graphs G and H are 0.9972 and 0.9985 respectively their equations generated from the graphs are y = 0.0018x + 3.3984 for graph G and y = 0.0034x + 3.3684 for graph H.

The above equations generated from the graphs were used to calculate the electron densities (ED) of the tissue equivalent materials selected for the research work. Table 4.4 summarizes the equations which have been grouped into positive HU (denser than water) and negative values which are less dense compared with water at the voltages that the scans were done.

4.4. HOUNSFIELD UNIT (HU), ELECTRON DENSITY AND RELATIVE ELECTRON DENSITIES (rED) OF THE SELECTED MATERIALS.

The results from Table4.4 indicate that the Hounsfield Units for Vegetable (Frytol) Oil and Sodium Hydroxide (NaOH) were higher than water, which serves as the standard reference medium in radiotherapy. Conversely, the Hounsfield Units for Total Quartz engine oil (SAE 15W-40) and Air were lower than the reference medium. Table 4.7 provided below represents the electron densities of selected materials at various kilovoltages and also, Table 4.8 provides averages densities with their standard deviations and relative electron densities of the selected materials.

Table 4. 4: Hounsfield Units of the selected materials at the various kilovoltages

		HU			
INSERTS	**MATERIALS**	**80 kV**	**100 kV**	**120 kV**	**140 kV**
062A-08	Frytol	114.439	70.285	58.615	20.03
062A-09	NaOH	74.906	100.272	97.973	48.207
062A-11	SAE 15W-40	-87.881	-100.208	-90.733	-86.088
062A-05	Air	-458.225	-479.88	-481.013	-465.86

Table 4. 5: Electron Densities of selected materials at various kilovoltages (kVp)

		HU			
INSERTS	**MATERIALS**	**80 kV**	**100 kV**	**120 kV**	**140 kV**
062A-08	Frytol	3.405	3.508	3.499	3.434
062A-09	NaOH	3.416	3.55	3.566	3.485
062A-11	SAE 15W-40	3.011	3.046	3.042	3.076
062A-05	Air	2.016	1.755	1.754	1.784

Table 4. 6: Average densities with their standard deviations and relative electron densities of the selected materials.

INSERTS	**MATERIALS**	**ED ($\times 10^{23}$)**	**Red**
062A-08	Frytol	3.462 ± 0.050	1.036
062A-09	NaOH	3.504 ± 0.068	1.049
062A-11	SAE 15W-40	3.044 ± 0.027	0.911
062A-05	Air	2.016 ± 0.127	0.547

Table 4.9 contains the results of the selected materials which were compared with the known tissues inserted in the electron density phantom. This comparison was done to determine the tissues that are equivalent to the selected materials. From Table 4.9, the relative electron densities of the Liver and NaOH were found to be in the same range, making NaOH equivalent to the Liver. Muscle and vegetable (Frytol) oil from the table shows that they are in the same range based on their relative electron densities. Adipose with a relative electron density (rED) of 0.949 is also equivalent to Total Quartz (SAE 15W-40) engine oil with a relative electron density of 0.911 and Lungs (Exhale) is equivalent to Air with relative electron densities (rED) of 0.489 and 0.547 respectively.

In medical treatments like brachytherapy, where accurate radiation targeting is very key, relative electron density (rED) is preferred over absolute electron density when comparing how tissues interact with radiation. Relative electron density (rED) helps us compare different tissues and materials by using water (assigned a rED of 1.0) as a standard reference. Water is ideal to use as a baseline because, its properties are similar to those of soft tissues, which makes it a universal standard in medical physics. By comparing everything to water, relative electron density (rED) considers each tissue's specific chemical makeup which allows for easy comparison between other tissues behaviour (Sarfehnia et al., 2007).

Using rED is helpful in brachytherapy, where tissue differences can strongly affect how radiation interacts with the body. With rED, treatment planning systems can easily and accurately adjust the radiation dose to account for various tissue types like bone, muscle, and fats. This ensures that, each tissue receives the correct amount of radiation (Zeman et al., 2020).

"Measured doses were consistently lower than the calculated values for dense materials, suggesting that the treatment planning system may slightly overestimate dose in high-density regions. This difference is likely due to tissue heterogeneity and beam-hardening effects. However, the deviations remained within acceptable limits, indicating no significant dosimetric error.

Table 4. 7: Comparism between the rED of the known phantom tissues and the selected materials.

PHANTOM TISSUE	rED	SELECTED MATERIAL	rED
Liver	1.053	NaOH	1.049
Muscle	1.043	Vegetable (Frytol) oil	1.036
Adipose	0.949	SAE 15W-40	0.911
Lungs (Exhale)	0.489	Air	0.547

4.5. HOMOGENEOUS MEASUREMENT OF THE SELECTED MATERIALS.

By analyzing materials such as Frytol oil and NaOH against water, as shown in Table 4.10, the results highlighted how different materials affect dose distribution patterns around the radiation source.

Table 4. 8: Results obtained from the homogeneous measurement of the selected materials

Materials	Position	Readings (nC)	Mcor (nC)	Dmeas. (Gy)	Dcal (Gy)	% Dose Difference
AIR	2.5	29.217	29.441	1.420	1.40	1.43
	4.5	20.941	21.268	0.931	0.93	-0.11
	7.7	3.471	3.489	0.168	0.18	-6.52
	10.0	2.437	2.447	0.118	0.12	-4.60
	12.6	1.268	1.270	0.061	0.06	2.10
WATER						
	2.5	24.093	24.222	1.168	1.40	-16.56
	4.5	16.009	16.169	0.780	0.93	-16.15
	7.7	3.073	3.110	0.150	0.18	-16.66
	10.0	2.092	2.128	0.103	0.12	-14.49
	12.6	0.983	1.005	0.048	0.06	-19.20
NaOH						
	2.5	22.717	23.104	1.114	1.40	-20.41
	4.5	15.152	15.410	0.743	0.93	-20.09
	7.7	3.048	3.096	0.149	0.18	-17.03
	10.0	2.055	2.084	0.101	0.12	-16.25
	12.6	0.933	0.946	0.046	0.06	-23.95
SAE 15W-40						
	2.5	24.863	25.176	1.214	1.40	-13.27
	4.5	12.460	12.616	0.608	0.93	-34.57
	7.7	3.016	3.053	0.147	0.18	-18.20
	10.0	2.232	2.259	0.109	0.12	-9.19
	12.6	0.979	0.991	0.048	0.06	-20.38

FRYTOL OIL						
	2.5	24.640	24.945	1.203	1.40	-14.06
	4.5	16.348	16.544	0.798	0.93	-14.20
	7.7	3.082	3.120	0.151	0.18	-16.39
	10.0	2.105	2.130	0.103	0.12	-14.38
	12.6	1.001	1.011	0.049	0.06	-18.72

Table 4.10 presents the charges detected by the ionization chamber using the PTW UNIDOS electrometer, with readings corrected for air density. Some factors like temperature and humidity can affects the air density and may impact the accuracy of the dose measured.

For air, the percentage dose differences ranged from 0.11% to 6.52%, while for water, NaOH, Total Quartz (SAE 15W-40), and Frytol oil, the ranges were 14.49% to 19.20%, 16.25% to 23.95%, 9.19% to 34.57%, and 14.06% to 18.76%, respectively. The results revealed a close agreement between the measured and calculated doses for air across the different compartments, but this agreement was not observed for the other materials. This discrepancy can be attributed to the physical densities of the materials. It is well-known that denser materials tend to absorb more radiation compared to low-density materials like air, which allow radiation to pass through more easily (Zabihzadeh et al., 2013; Wu et al., 2014).

Another factor influencing these observations is the atomic number of the materials, which affects the measured dose distribution (Mann-Krzisnik et al., 2018). Materials with higher atomic numbers contain heavier atoms that can absorb and scatter radiation more

effectively. In low-density materials such as air, scattering is the predominant interaction mechanism, while in denser materials, absorption is more significant.

Electron density, defined as the number of electrons per unit volume in a material, also plays a critical role in dose distribution during brachytherapy. Materials with higher electron densities, like NaOH, interact more with radiation, resulting in increased scattering and absorption that alter the dose pattern. The "attenuation coefficient," a measure of how easily radiation is absorbed or scattered in a material, further explains these variations (Su et al., 2019).

Water, often used as a standard due to its similarity to human tissue, provides a baseline for comparison. In radiotherapy, accuracy of dose is stated as 5% but some of the dense materials in this study is much higher than the percentage stated. This suggests that, the algorithm may overestimate dose in high-density areas due to tissue heterogeneity and beam hardening effects.

4.6 CORRELATION BETWEEN DOSE MEASURED AND THE DISTANCE S FROM THE SOURCE.

The graphs presented in figures 4.3 to 4.7 are polynomic relationship between dose measured and the distances from the source to each of the medium for Air, Water, NaOH, SAE 15W-40 and Vegetable (Frytol) oil respectfully.

At larger distances (8–12 cm), the measured dose decreased more rapidly compared to shorter distances (2–6 cm). This is mainly due to the inverse square law, attenuation, and reduced scatter contribution at greater depths, resulting in lower detector readings.

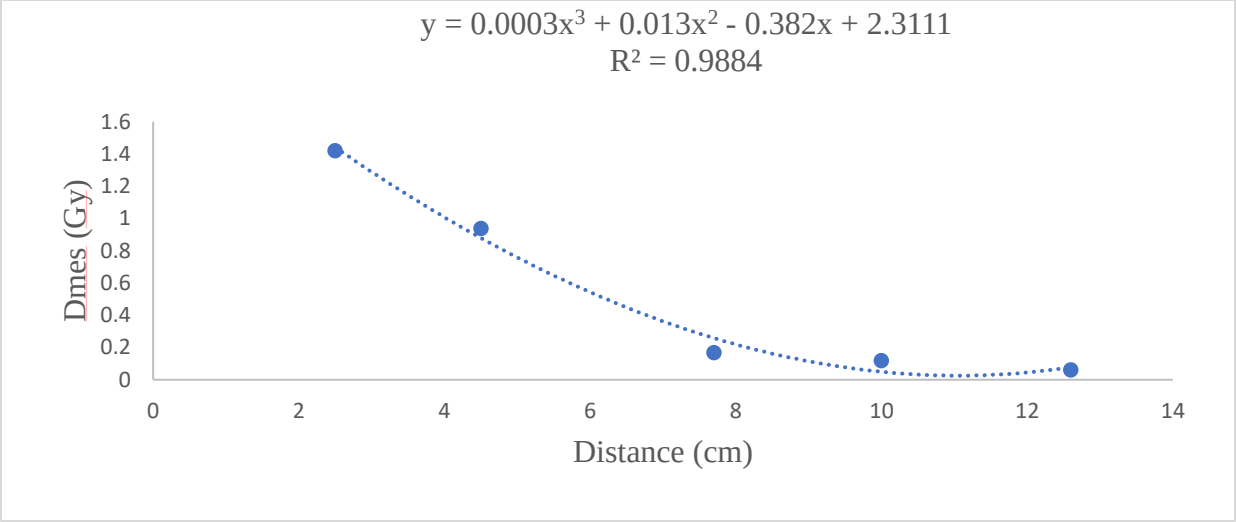

Figure 4. 3: Polynomic relationship between dose measured and distance in homogeneous measurement for Air.

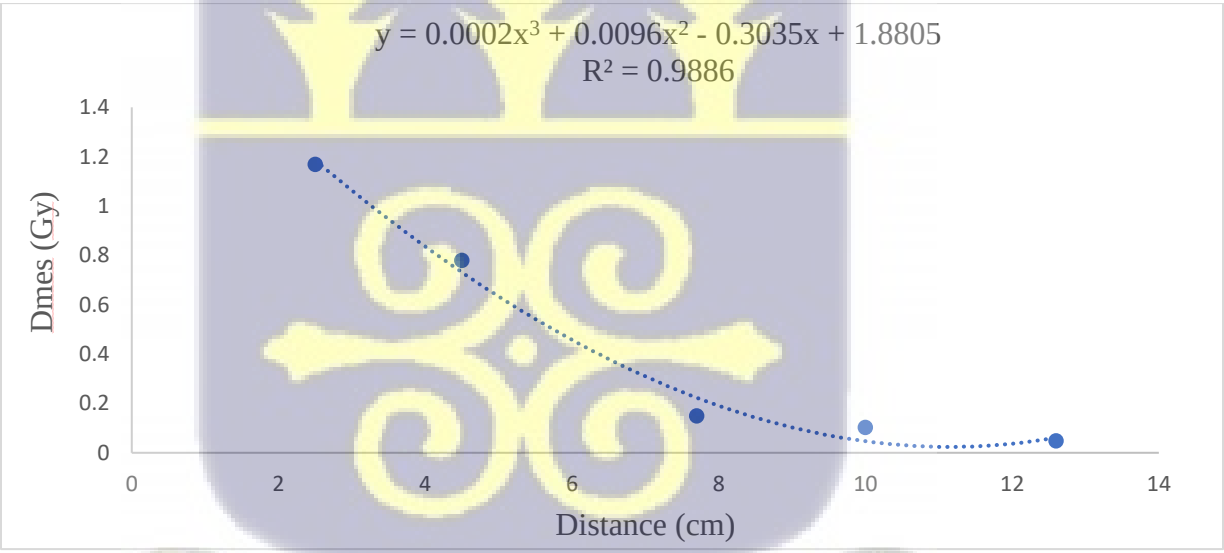

Figure 4. 4: Polynomic relationship between dose measured and distance in homogeneous measurement Water.

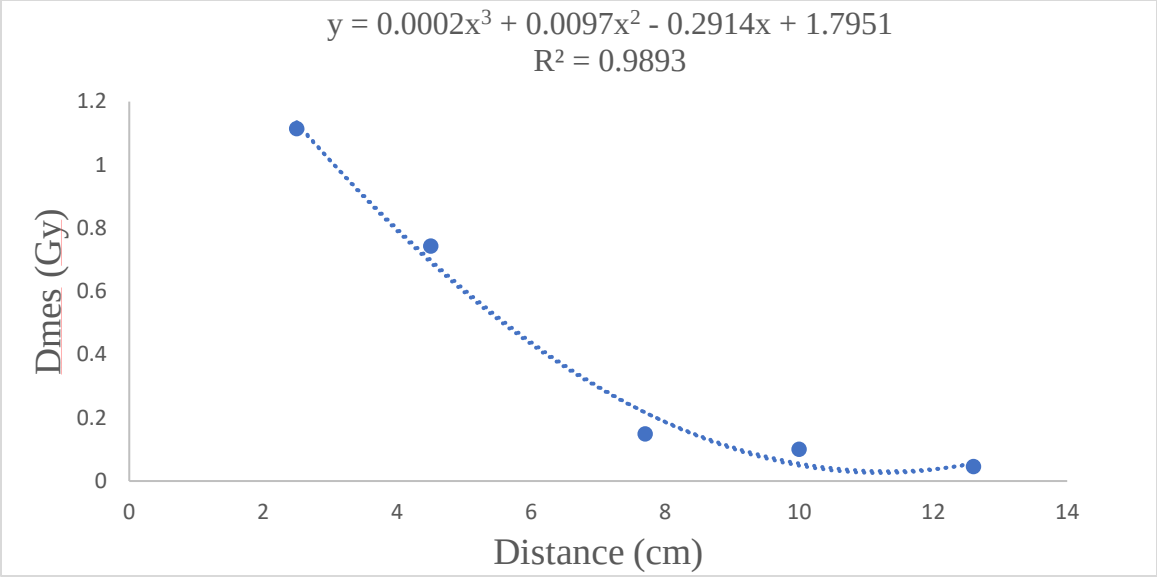

Figure 4. 5: Polynomic relationship between dose measured and distance in homogeneous measurement for NaOH.

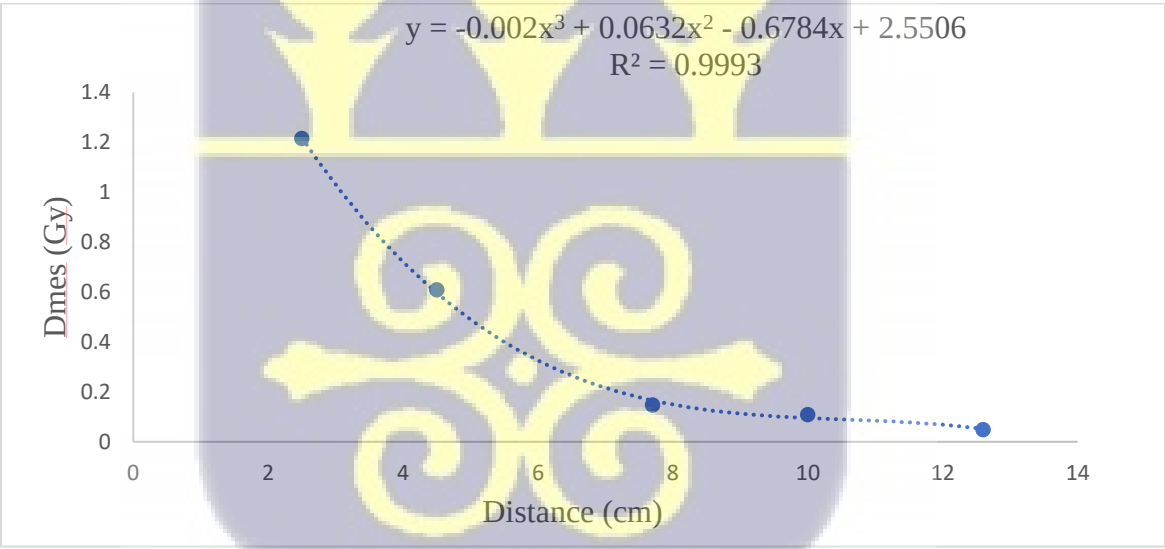

Figure 4. 6: Polynomic relationship between dose measured and distance in homogeneous measurement for SAE 15W-40.

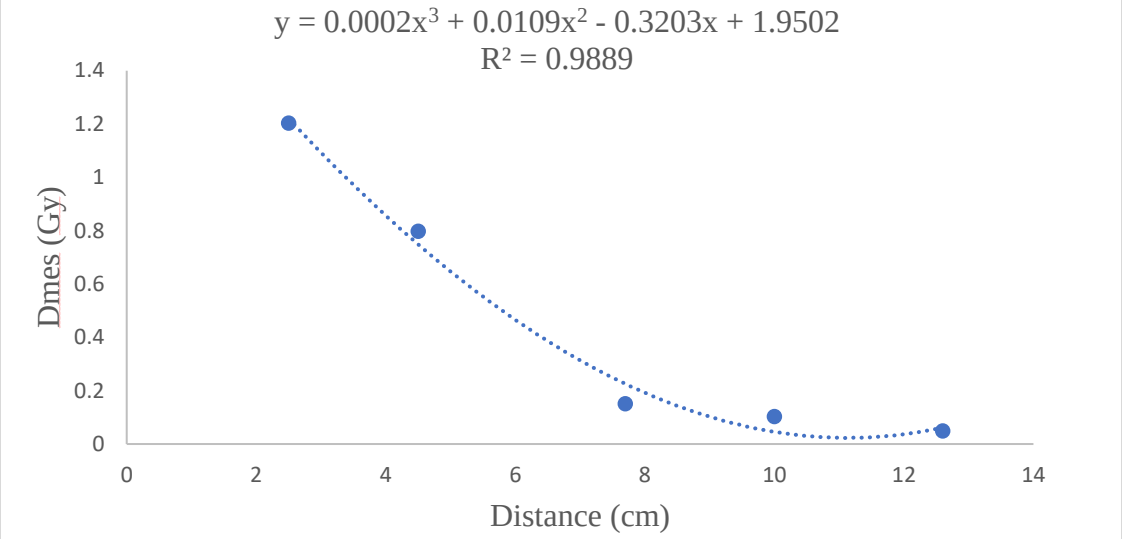

Figure 4. 7: Polynomic relationship between dose measured and distance in homogeneous measurement for Vegetable (Frytol) oil.

In brachytherapy, a graph of dose measured versus distance explains how radiation spreads out from the source. The curves in the graphs above shows a sharp drop in dose as the distance increases from the source and this fall follows the inverse square law as emphasized by Rivard et al. (2004).

4.7 HETEROGENEOUS MEASUREMENTS OF THE SELECTED MATERIALS.

Table 4.11 presents the results of heterogeneous measurement of the selected materials and analyzing the results from Table 4.11 shows a unique trend which indicates that, the position of each material differs and affects how the radiations are distributed in all the six permutations.

Table 4. 9: Heterogeneous measurement of the selected materials.

Materials	Position (cm)	Medium	Readings (nC)	Mcor (nC)	Dmeas (Gy)	Dcal (Gy)	% Dose Difference
Frytol oil	2.5		42.523	43.187	2.083	2.00	4.15
SAE 15W-40	7.7		8.819	8.957	0.432	0.46	-6.09
NaOH	12.6		3.429	3.483	0.168	0.19	-11.59
Frytol oil	2.5		43.21	43.905	2.118	2.00	5.88
NaOH	7.7		8.924	9.054	0.437	0.46	-5.07
SAE 15W-40	12.6		3.264	3.309	0.160	0.19	16.00
SAE 15W-40	2.5		40.97	41.554	2.004	2.00	0.21
Frytol oil	7.7		8.746	8.875	0.428	0.46	-6.95
Na0H	12.6		3.437	3.488	0.68	0.19	-11.45
SAE 15W-40	2.5		40.223	40. 827	1.969	2.00	-1.55
NaOH	7.7		8.758	8.758	0.422	0.46	-8.18
Frytol oil	12.6		3.269	3.313	0.151	0.19	-15.90

NaOH	2.5	42.133	42.839	2.066	2.00	3.31
Frytol oil	7.7	8.750	8.885	0.428	0.46	-6.85
SAE 15W-40	12.6	3.335	3.386	0.163	0.19	-14.05
NaOH	2.5	42.107	42.841	2.066	2.00	3.31
SAE 15W 40	7.7	8.466	8.606	0.415	0.46	-9.76
Frytol	12.6	3.335	3.383	0.163	0.19	-14.11

For instance, comparing permutation 1 and 2, when the position of Frytol oil was maintained in compartment 1 which was very close to the source, the difference in the measurement of the dose as presented in percentage dose difference was small compared with SAE 15W-40 and NaOH when their positions were changed in each of the medium.

This trend is consistent throughout the measurement done in table 4.11 and this can be attributed to many factors including temperature, dose calculation algorithms dedicated to brachytherapy which does not account for heterogeneities. Other factors such as the scattering and absorption, lack of back scatter, volume averaging effects among others may contribute to the trends examined from the table.

Using the positions of the materials in any of the medium or permutations, another observation made was that, there is a huge fall between the materials closed to the source and the medium (materials) that is far apart from the source and it run through all the six permutations. This huge fall is also clearly expressed in a percentage dose difference which

is an evident of the inverse square law. Although this huge fall may not be usual in brachytherapy treatment, the idea that, as distance increases in a heterogeneous medium, dose distribution becomes affected is also evident and the effects of absorption and scattering on dose distribution in heterogeneous system may affect treatment outcomes.

The percentage dose difference presented in Table 4.11 was used to evaluate the TPS calculated dose and the measured dose. From table, the location of the inhomogeneities from the source is one of the factors that influences the difference between the measured dose and the TPS calculated dose. According DeWerd et al. (2011), in brachytherapy, as proposed by the AAPM, the accepted range for percentage dose difference is within (±5%) and percentages outside the range may have significant effects on the outcome. The percentage dose difference indicates how the measured dose deviates from the TPS calculated dose and therefore, Percentage dose difference above the accepted range indicates that, the delivered (Dmeas.) dose is higher than the planned (Dcal.) dose. This can cause overdose to the affected and the surrounding healthy tissues.

Percentage dose difference below the accepted range indicates that, the delivered (Dmeas.) dose is lower than the planned (Dcal.) dose. This can also lead to underdose to the affected and the surrounding healthy tissues and the treatment may not be efficient. The discrepancies between the measured and the calculated doses, and the large distance from the source can be attributed to the degeneration of TG43 formalism at distances greater than 5cm (Roussakis et al., 2024).

Some of the dense materials in this study in much higher than 5% accuracy stated in brachytherapy. This suggests that, the algorithm may overestimate dose in high-density areas due to tissue heterogeneity and beam-hardening effects.

4.8 SEMI EMPIRICAL EQUATION

Figure 4.8 is an illustration of a polynomic relationship of a semi empirical equation generated between the measured dose and TPS calculated dose and from the graph. The equation developed is given as $y = 0.0002x^3 + 0.0127x^2 - 0.3716x + 2.2666$. Where y and x are dose measured and distance from the source respectively. The equation is use to estimate the dose deposition in each medium. To estimate the dose deposited in each of a heterogeneous medium, the polynomic equation developed from equation 4 takes the general polynomial form as $D = ax^3 + bx^2 + Cx + K$ eqn 5. Where, a, b, c and K are constants in eqn 4 and X = rED of the materials.

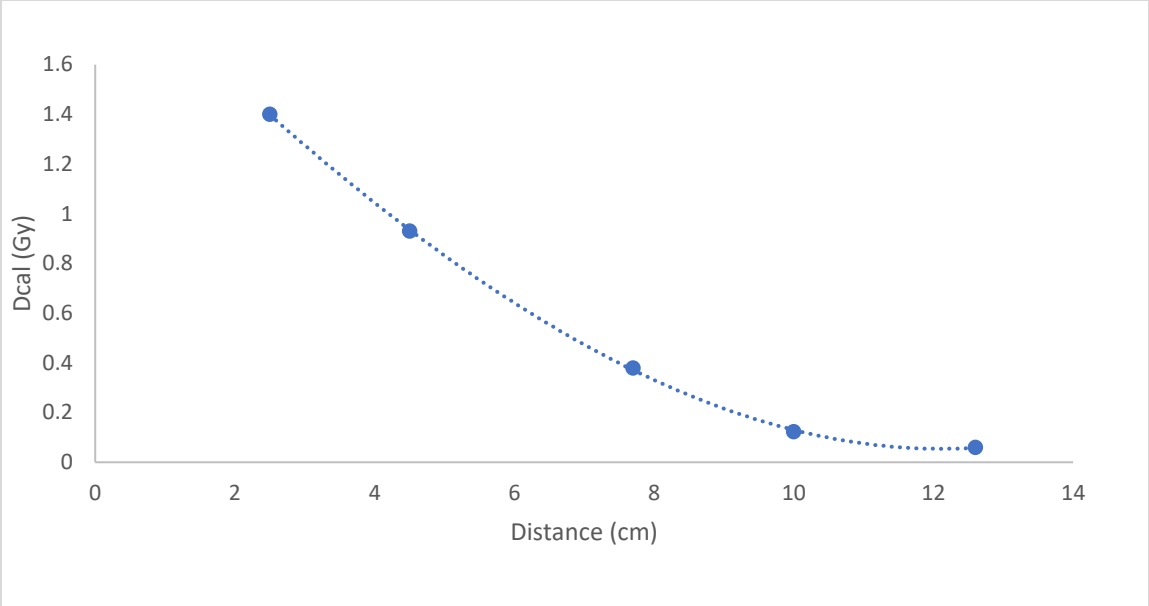

Figure 4.8: An illustration of a polynomic relationship between the measured dose and TPS calculated dose.

CHAPTER FIVE

CONCLUSION AND RECOMMENDATIONS

5.0 OVERVIEW

This chapter provides a comprehensive conclusion on the research topic "Effects of Tissue Heterogeneities on Dose Estimation in Brachytherapy". It also includes the limitations of the study as well as the recommendations for future studies.

5.1 CONCLUSION

In this study, the impact of tissue heterogeneities on dose distribution was thoroughly investigated to improve treatment accuracy and outcomes. The research highlighted the significant role tissue density variations play in dose estimation during brachytherapy and explored ways to mitigate their effects.

Key findings revealed that denser tissues, such as bone and liver, absorb more radiation, while less dense tissues, like lungs or adipose, allow greater scattering. Similarly, material equivalencies, such as Sodium Hydroxide (NaOH) for liver and Frytol oil for muscle, were identified, offering potential for more realistic tissue simulations in radiotherapy. The study also demonstrated how the attenuation coefficient and radiation energy influence dose distribution, with dense materials favoring absorption and lighter ones promoting scattering.

Furthermore, the research emphasized the importance of material positioning relative to the radiation source. Dose deviations, influenced by the inverse square law and TG-43 formalism limitations, highlighted discrepancies between measured and calculated doses, particularly beyond 5 cm. These deviations, if unaccounted for, could result in underdosing or overdosing, affecting both healthy tissues and treatment efficacy.

The study hence emphasizes the necessity of incorporating tissue heterogeneities and precise material positioning into dose planning protocols to ensure accurate and effective brachytherapy treatments.

5.2 RECOMMENDATIONS

To the Scientific Community & Medical Physicist Professionals, it is recommended that, the study can be repeated for materials with vast electron densities and with more materials within the scientific community.

It is recommended to the research facility that; the semi empirical equation should be tested on a complex source geometry before it is used for patient treatment.

REFERENCES

Adelnia, A., & Fatehi, D. (2016). Estimation and evaluation of tissue inhomogeneity effect on dose distribution for high dose rate Iridium 192 source using Monte Carlo Simulation and film dosimetry. *Journal of Nuclear Medicine & Radiation Therapy*, *07*(06).

Akhavanallaf, A., Mohammadi, R., Shiri, I., Salimi, Y., Arabi, H., & Zaidi, H. (2021). Personalized brachytherapy dose reconstruction using deep learning. *Computers in Biology and Medicine*, *136*, 104755.

Alberga, J. M., Vosselman, N., Korfage, A., Delli, K., Witjes, M. J. H., Raghoebar, G. M., & Vissink, A. (2020). What is the optimal timing for implant placement in oral cancer patients? A scoping literature review. *Oral Diseases*, *27*(1), 94–110.

Åström, L., Grusell, E., Sandin, F., Turesson, I., & Holmberg, L. (2018). Two decades of high-dose-rate brachytherapy with external beam radiotherapy for prostate cancer. *Radiotherapy and Oncology*, *127*(1), 81–87. https://doi.org/10.1016/j.radonc.2017.12.025

Balgobind, B. V., Koedooder, K., Zúñiga, D. O., Fajardo, R. D., Rasch, C. R. N., & Pieters, B. R. (2015). A review of the clinical experience in pulsed dose rate brachytherapy. *The British Journal of Radiology/British Journal of Radiology*, *88*(1055), 20150310.

Barry, R., Forde, E., & Barrett, S. (2021). Improving organ at risk sparing in oropharyngeal treatment planning by increasing target dose heterogeneity: A feasibility study. *Medical Dosimetry*, *46*(3), 304–309.

Bauer, J., Sommerer, F., Mairani, A., Unholtz, D., Farook, R., Handrack, J., Frey, K., Marcelos, T., Tessonnier, T., Ecker, S., Ackermann, B., Ellerbrock, M., Debus, J., & Parodi, K. (2014). Integration and evaluation of automated Monte Carlo simulations in the clinical practice of scanned proton and carbon ion beam therapy. *Physics in Medicine & Biology/Physics in Medicine and Biology*, *59*(16), 4635–4659.

Berg, S., Cole, A. P., Krimphove, M. J., Nabi, J., Marchese, M., Lipsitz, S. R., Noldus, J., Choueiri, T. K., Kibel, A. S., & Trinh, Q. (2019). Comparative Effectiveness of Radical Prostatectomy Versus External Beam Radiation Therapy Plus Brachytherapy in Patients with High-risk Localized Prostate Cancer. *European Urology*, *75*(4), 552–555.

Bocan, K. N., Mickle, M. H., & Sejdic, E. (2018). Simulating, modelling, and sensing variable tissues for wireless implantable medical devices. *IEEE Transactions on Microwave Theory and Techniques*, *66*(7), 3547–3556.

Brown, J. S., Amend, S. R., Austin, R. H., Gatenby, R. A., Hammarlund, E. U., & Pienta, K. J. (2023). Updating the definition of cancer. *Molecular Cancer Research*, *21*(11), 1142–1147. https://doi.org/10.1158/1541-7786.mcr-23-0411

Chargari, C., Deutsch, E., Blanchard, P., Gouy, S., Martelli, H., Guérin, F., Dumas, I., Bossi, A., Morice, P., Viswanathan, A. N., & Haie-Meder, C. (2019). Brachytherapy: An overview for clinicians. *CA a Cancer Journal for Clinicians*, *69*(5), 386–401. https://doi.org/10.3322/caac.21578

Chen, X., Men, K., Li, Y., Yi, J., & Dai, J. (2018). A feasibility study on an automated method to generate patient-specific dose distributions for radiotherapy using deep learning. *Medical Physics on CD-ROM/Medical Physics*, *46*(1), 56–64.

Chiang, B., Schnell, E., Hibbitts, K., Herman, T., & Ahmad, S. (2020). Dosimetric analysis and comparison of volumetric-modulated arc therapy versus intensity-modulated radiation therapy for liver carcinoma. *Journal of Radiotherapy in Practice*, *21*(1), 138–140.

Chopra, K. L., Leo, P., Kabat, C., Rai, D. V., Avadhani, J. S., Kehwar, T. S., & Sethi, A. (2018). Evaluation of dose calculation accuracy of treatment planning systems in the presence of tissue heterogeneities. *Therapeutic Radiology and Oncology*, *2*, 28.

Cicero, M. X., Adelgais, K., Hoyle, J. D., Lyng, J. W., Harris, M., Moore, B., & Gausche-Hill, M. (2020). Medication Dosing Safety for Pediatric Patients: Recognizing Gaps, Safety Threats, and Best Practices in the Emergency Medical Services Setting. A Position Statement and Resource Document from NAEMSP. *Prehospital Emergency Care*, *25*(2), 294–306.

Cropp, R. J., Seslija, P., Tso, D., & Thakur, Y. (2013). Scanner and kVp dependence of measured CT numbers in the ACR CT phantom. *Journal of Applied Clinical Medical Physics*, *14*(6), 338–349. https://doi.org/10.1120/jacmp.v14i6.4417

Crowe, S. B., Kairn, T., Middlebrook, N., Hill, B., Christie, D. R. H., Knight, R. T., Kenny, J., Langton, C. M., & Trapp, J. V. (2013). Retrospective evaluation of dosimetric quality for prostate carcinomas treated with 3D conformal, intensity

modulated and volumetric modulated arc radiotherapy. *Journal of Medical Radiation Sciences*, *60*(4), 131–138. https://doi.org/10.1002/jmrs.24

Davé, B. A., Jaber, C., Leader-Cramer, A., Higgins, N., Mueller, M., Lewicky-Gaupp, C., & Kenton, K. (2016). Effect of anesthesia type on perioperative outcomes with a midurethral sling. *International Urogynecology Journal*, *27*(9), 1327–1332.

Deng, X., Wu, H., Gao, F., Su, Y., Li, Q., Liu, S., & Cai, J. (2017). Brachytherapy in the treatment of breast cancer. *International Journal of Clinical Oncology*, *22*(4), 641–650. https://doi.org/10.1007/s10147-017-1155-5

DeWerd, L. A., Ibbott, G. S., Meigooni, A. S., Mitch, M. G., Rivard, M. J., Stump, K. E., Thomadsen, B. R., & Venselaar, J. L. M. (2011). A dosimetric uncertainty analysis for photon-emitting brachytherapy sources: Report of AAPM Task Group No. 138 and GEC-ESTRO. *Medical Physics*, *38*(2), 782–801. https://doi.org/10.1118/1.3533720

Dupoiron, D., Douillard, T., & Carvajal, G. (2020). The usefulness of Imaging for Intrathecal Drug Delivery Systems: An update. *Medical Research Archives*, *8*(7).

Edher, F., & Nguyen, C. T. (2018). Short dental implants: A scoping review of the literature for patients with head and neck cancer. ˜ *the œ Journal of Prosthetic Dentistry/˜ the œ Journal of Prosthetic Dentistry*, *119*(5), 736–742.

Enger, S. A., Vijande, J., & Rivard, M. J. (2020). Model-Based Dose Calculation Algorithms for brachytherapy dosimetry. *Seminars in Radiation Oncology*, *30*(1), 77–86.

Enger, S. A., Vijande, J., & Rivard, M. J. (2019). Model-Based Dose calculation Algorithms for brachytherapy dosimetry. *Seminars in Radiation Oncology*, *30*(1), 77–86. https://doi.org/10.1016/j.semradonc.2019.08.006

Esteva-Socias, M., Artiga, M., Bahamonde, O., Belar, O., Bermudo, R., Castro, E., Escámez, T., Fraga, M., Jauregui-Mosquera, L., Novoa, I., Peiró-Chova, L., Rejón, J., Ruiz-Miró, M., Vieiro-Balo, P., Villar-Campo, V., Zazo, S., Rábano, A., & Villena, C. (2019). In search of an evidence-based strategy for quality assessment of human tissue samples: report of the tissue Biospecimen Research Working Group of the Spanish Biobank Network. *Journal of Translational Medicine*, *17*(1).

Famulari, G., Renaud, M., Poole, C. M., Evans, M. D. C., Seuntjens, J., & Enger, S. A. (2018). RapidBrachyMCTPS: a Monte Carlo-based treatment planning system for brachytherapy applications. *Physics in Medicine & Biology/Physics in Medicine and Biology*, *63*(17), 175007.

Fan, J., Wang, J., Chen, Z., Hu, C., Zhang, Z., & Hu, W. (2018). Automatic treatment planning based on three-dimensional dose distribution predicted from deep learning technique. *Medical Physics on CD-ROM/Medical Physics*, *46*(1), 370–381.

Ferranti, E., Andres, L., Denoon-Stevens, S. P., Melgaço, L., Oberling, D., & Quinn, A. (2020). Operational challenges and mega sporting events legacy: the case of BRT systems in the global South. *Sustainability*, *12*(4), 1609.

Fogliata, A., De Rose, F., Stravato, A., Reggiori, G., Tomatis, S., Scorsetti, M., & Cozzi, L. (2018). Evaluation of target dose inhomogeneity in breast cancer treatment due to tissue elemental differences. *Radiation Oncology*, *13*(1).

Fonseca, G. P., Johansen, J. G., Smith, R. L., Beaulieu, L., Beddar, S., Kertzscher, G., Verhaegen, F., & Tanderup, K. (2020). In vivo dosimetry in brachytherapy: Requirements and future directions for research, development, and clinical practice. *Physics and Imaging in Radiation Oncology*, *16*, 1–11.

Gill, B. S., Kim, H., Houser, C. J., Kelley, J. L., Sukumvanich, P., Edwards, R. P., Comerci, J. T., Olawaiye, A. B., Huang, M., Courtney-Brooks, M., & Beriwal, S. (2015). MRI-Guided High–Dose-Rate Intracavitary brachytherapy for treatment of cervical Cancer: the University of Pittsburgh Experience. *International Journal of Radiation Oncology, Biology, Physics*, *91*(3), 540–547.

Glide-Hurst, C. K., & Chetty, I. J. (2014). Improving radiotherapy planning, delivery accuracy, and normal tissue sparing using cutting-edge technologies. *PubMed*, *6*(4), 303–318. https://doi.org/10.3978/j.issn.2072-1439.2013.11.10

Grégoire, V., Guckenberger, M., Haustermans, K., Lagendijk, J. J. W., Ménard, C., Pötter, R., Slotman, B. J., Tanderup, K., Thorwarth, D., Van Herk, M., & Zips, D. (2020). Image guidance in radiation therapy for better cure of cancer. *Molecular Oncology*, *14*(7), 1470–1491.

Han, D. Y., Webster, M. J., Scanderbeg, D. J., Yashar, C., Choi, D., Song, B., Devic, S., Ravi, A., & Song, W. Y. (2014). Direction-Modulated Brachytherapy for High-Dose-Rate Treatment of Cervical Cancer. i: Theoretical design. *International Journal of Radiation Oncology, Biology, Physics*, *89*(3), 666–673.

Hasani, M., Mohammadi, K., Ghorbani, M., Gholami, S., & Knaup, C. (2019). A Monte Carlo evaluation of dose distribution of commercial treatment planning systems in

heterogeneous media. *Journal of Cancer Research and Therapeutics/Journal of Cancer Research and Therapeutics*, *15*(Suppl 1), S127–S134.

Healy, B., Van Der Merwe, D., Christaki, K., & Meghzifene, A. (2016). Cobalt-60 Machines and Medical Linear Accelerators: competing technologies for external beam radiotherapy. *Clinical Oncology*, *29*(2), 110–115. https://doi.org/10.1016/j.clon.2016.11.002

Holschneider, C. H., Petereit, D. G., Chu, C., Hsu, I., Ioffe, Y. J., Klopp, A. H., Pothuri, B., Chen, L., & Yashar, C. (2019). Brachytherapy: A critical component of primary radiation therapy for cervical cancer. *Gynecologic Oncology*, *152*(3), 540–547.

Huang, Y., Li, S., Yue, H., Wang, M., Hu, Q., Wang, H., Li, T., Li, C., Wu, H., & Zhang, Y. (2019). Impact of nominal photon energies on normal tissue sparing in knowledge-based radiotherapy treatment planning for rectal cancer patients. *PloS One*, *14*(3), e0213271.

Hueso-González, F., Vijande, J., Ballester, F., Perez-Calatayud, J., & Siebert, F. (2015). A simple analytical method for heterogeneity corrections in low dose rate prostate brachytherapy. *Physics in Medicine & Biology/Physics in Medicine and Biology*, *60*(14), 5455–5469.

Jamadagni, S., Ponni, A., & P, R. (2024). Dosimetric comparison of intra-cavitary brachytherapy technique with free-hand (intra-cavitary + interstitial) technique in cervical cancer. *Journal of Contemporary Brachytherapy*, *16*(1), 28–34. https://doi.org/10.5114/jcb.2024.135629

Katsarou, E., Karava, K., Stamatelatos, I. E., & Kalef-Ezra, J. (2019). Dose Distribution near Tissue In-homogeneities in Megavoltage Radiation Therapy. *HNPS Advances in Nuclear Physics*, *23*, 94.

Khosroabadi, M., Farhood, B., Ghorbani, M., Hamzian, N., Moghaddam, H. R., & Davenport, D. (2016). Tissue composition effect on dose distribution in neutron brachytherapy/neutron capture therapy. *Reports of Practical Oncology and Radiotherapy*, *21*(1), 8–16.

Kim, K. J., Kim, D. H., Lee, J. I., Choi, B. K., Han, I. H., & Nam, K. H. (2019). Hounsfield units on lumbar computed tomography for predicting regional bone mineral density. *Open Medicine*, *14*(1), 545–551. https://doi.org/10.1515/med-2019-0061

King, M. T., Keyes, M., Frank, S. J., Crook, J. M., Butler, W. M., Rossi, P. J., Cox, B. W., Showalter, T. N., Mourtada, F., Potters, L., Stock, R. G., Kollmeier, M. A., Zelefsky, M. J., Davis, B. J., Merrick, G. S., & Orio, P. F. (2021). Low dose rate brachytherapy for primary treatment of localized prostate cancer: A systemic review and executive summary of an evidence-based consensus statement. *Brachytherapy*, *20*(6), 1114–1129.

Knoll, I. M., Quevedo, A., & Sánchez, M. S. A. (2022). Applications of simulation codes based on Monte Carlo method for radiotherapy. In *IntechOpen eBooks*.

Landry, G., Gaudreault, M., Van Elmpt, W., Wildberger, J. E., & Verhaegen, F. (2016). Improved dose calculation accuracy for low energy brachytherapy by optimizing dual energy CT imaging protocols for noise reduction using sinogram-affirmed iterative reconstruction. *Zeitschrift Für Medizinische Physik*, *26*(1), 75–87.

Lesperance, M., Martinov, M., & Thomson, R. M. (2014). Monte Carlo dosimetry for 103Pd, 125I, and 131Cs ocular brachytherapy with various plaque models using an eye phantom. *Medical Physics on CD-ROM/Medical Physics*, *41*(3). https://doi.org/10.1118/1.4864474

Mann-Krzisnik, D., Verhaegen, F., & Enger, S. A. (2018). The influence of tissue composition uncertainty on dose distributions in brachytherapy. *Radiotherapy and Oncology*, *126*(3), 394–410. https://doi.org/10.1016/j.radonc.2018.01.007

Mariotti, A. (2021). Effect of pFNA internal fixation of senile fracture in maxillofacial injuries. *Science Progress and Research*, *1*(3), 255–259. https://doi.org/10.52152/spr/2021.121

Mendez, L. C., & Morton, G. C. (2018). High dose-rate brachytherapy in the treatment of prostate cancer. *Translational Andrology and Urology*, *7*(3), 357–370.

Molinari, C., Marisi, G., Passardi, A., Matteucci, L., De Maio, G., & Ulivi, P. (2018). Heterogeneity in colorectal cancer: a challenge for personalized medicine? *International Journal of Molecular Sciences*, *19*(12), 3733.

Montero, A. M. B., Souris, K., Sanchez-Parcerisa, D., Sterpin, E., & Lee, J. A. (2017). Performance of a hybrid Monte Carlo-Pencil Beam dose algorithm for proton therapy inverse planning. *Medical Physics on CD-ROM/Medical Physics*, *45*(2), 846–862.

Moran, B. J., Koroulakis, A., Decesaris, C., Braccioforte, M. H., Amin, N., & Agarwal, M. (2021). Long-term outcomes of a prospective randomized trial of 131Cs/125I permanent prostate brachytherapy. *Brachytherapy*, *20*(1), 38–43.

Morcos, M., Viswanathan, A. N., & Enger, S. A. (2021). On the impact of absorbed dose specification, tissue heterogeneities, and applicator heterogeneities on Monte Carlo-based dosimetry of Ir-192, Se-75, and Yb-169 in conventional and intensity-modulated brachytherapy for the treatment of cervical cancer. *Medical Physics on CD-ROM/Medical Physics*, *48*(5), 2604–2613.

Moreno-Barbosa, F., De Celis-Alonso, B., Moreno-Barbosa, E., Hernández-López, J. M., Geoghegan, T., & Ramos-Méndez, J. (2020). Monte Carlo simulation of the effect of magnetic fields on brachytherapy dose distributions in lung tissue material. *PloS One*, *15*(10), e0238704.

Morrill, S., Langer, M., Lane, R., & Rosen, I. (1994). Tissue heterogeneity effects in treatment plan optimization. *International Journal of Radiation Oncology*Biology*Physics*, *30*(3), 699–706. https://doi.org/10.1016/0360-3016(92)90958-k

Morton, G., McGuffin, M., Chung, H. T., Tseng, C., Helou, J., Ravi, A., Cheung, P., Szumacher, E., Liu, S., Chu, W., Zhang, L., Mamedov, A., & Loblaw, A. (2020). Prostate high dose-rate brachytherapy as monotherapy for low and intermediate risk prostate cancer: Efficacy results from a randomized phase II clinical trial of one fraction of 19 Gy or two fractions of 13.5 Gy. *Radiotherapy and Oncology*, *146*, 90–96.

Neph, R., Huang, Y., Yang, Y., & Sheng, K. (2019). DeepMCDOse: A deep learning method for efficient Monte Carlo Beamlet dose calculation by predictive denoising in MR-Guided radiotherapy. In *Lecture notes in computer science* (pp. 137–145).

Nikolayev, D., Joseph, W., Zhadobov, M., Sauleau, R., & Martens, L. (2019). Optimal radiation of Body-Implanted capsules. *Physical Review Letters*, *122*(10).

Njiki, C. D., Manyol, J. E. M. N., Yigbedeck, Y. E., Abou'ou, D. W., Yimele, B. C., & Sabouang, J. F. (2018). Assessment of Image Quality Parameters for Computed Tomography in the City of Yaoundé *Open Journal of Radiology*, *08*(01), 37–44. https://doi.org/10.4236/ojrad.2018.81005

Oh, K., Sengupta, B., Olanrewaju, A., Zhang, L., Nair, S. S., Mani, T., Palanisamy, M., KanduKuri, U. S., Netherton, T. J., Cardenas, C. E., Court, L. E., & Ford, E. C. (2023). Commissioning and dosimetric validation of a novel compensator-based Co-60 IMRT system for evaluating suitability to automated treatment planning. *Medical Physics*, *50*(7), 4466–4479. https://doi.org/10.1002/mp.16423

Paganetti, H. (2015). Relating proton treatments to Photon treatments via the Relative Biological Effectiveness—Should we revise current clinical practice? *International Journal of Radiation Oncology, Biology, Physics*, *91*(5), 892–894.

Park, H., Choi, H. J., Kim, J., & Min, C. H. (2018). Analysis of dose distribution according to the initial electron beam of the linear accelerator: a Monte Carlo study. *Bangsa'seon Bang'eo Haghoeji/Journal of Radiation Protection and Research/Bangsaseon Bang-eo Hakoeji*, *43*(1), 10–19.

Paro, A. D., Hossain, M., Webster, T. J., & Su, M. (2016). Monte Carlo and analytic simulations in nanoparticle-enhanced radiation therapy. *International Journal of Nanomedicine*, *Volume 11*, 4735–4741.

Paz, A. E. S., Baumann, K., Weber, U. A., Witt, M., Zink, K., Durante, M., & Graeff, C. (2021). Compensating for beam modulation due to microscopic lung heterogeneities in carbon ion therapy treatment planning. *Medical Physics on CD-ROM/Medical Physics*, *48*(12), 8052–8061.

Peppa, V., Pappas, E., Major, T., Takácsi-Nagy, Z., Pantelis, E., & Papagiannis, P. (2016). On the impact of improved dosimetric accuracy on head and neck high dose rate brachytherapy. *Radiotherapy and Oncology*, *120*(1), 92–97.

Pignol, J., Caudrelier, J., Crook, J., McCann, C., Truong, P., & Verkooijen, H. A. (2015). Report on the clinical outcomes of Permanent breast seed implant for Early-Stage Breast Cancers. *International Journal of Radiation Oncology, Biology, Physics*, *93*(3), 614–621.

Prisciandaro, J. I., Zhao, X., Dieterich, S., Hasan, Y., Jolly, S., & Al-Hallaq, H. A. (2020). Interstitial High-Dose-Rate Gynecologic Brachytherapy: Clinical workflow experience from three academic institutions. *Seminars in Radiation Oncology*, *30*(1), 29–38.

Qu, H., Han, D., Zhang, N., Mao, Z., & Cheng, G. (2021). Intracavitary/Interstitial applicator plus distal parametrial free needle interstitial brachytherapy in locally advanced cervical cancer: a dosimetric study. *Frontiers in Oncology*, *10*. https://doi.org/10.3389/fonc.2020.621347

Ravikumar, B., & Lakshminarayana, S. (2012). Determination of the tissue inhomogeneity correction in high dose rate Brachytherapy for Iridium-192 source. *Journal of Medical Physics*, *37*(1), 27. https://doi.org/10.4103/0971-6203.92717

Rivard, M. J., Coursey, B. M., DeWerd, L. A., Hanson, W. F., Huq, M. S., Ibbott, G. S., Mitch, M. G., Nath, R., & Williamson, J. F. (2004). Update of AAPM Task Group No. 43 Report: A revised AAPM protocol for brachytherapy dose calculations. *Medical Physics*, *31*(3), 633–674. https://doi.org/10.1118/1.1646040

Roussakis, Y., Antorkas, G., Georgiou, L., Strouthos, I., Karagiannis, E., Zamboglou, C., Ferentinos, K., Zamboglou, N., & Anagnostopoulos, G. (2024). Dosimetric comparison of AcurosTM BV and AAPM TG-43 formalism for interstitial iridium-192 high-dose-rate brachytherapy. *Journal of Contemporary Brachytherapy*, *16*(3), 211–218. https://doi.org/10.5114/jcb.2024.140893

Sarfehnia, A., Stewart, K., & Seuntjens, J. (2007). An absorbed dose to water standard for HDR I192r brachytherapy sources based on water calorimetry: Numerical and experimental proof-of-principle. *Medical Physics*, *34*(12), 4957–4961. https://doi.org/10.1118/1.2815941

Satpathy, M., Wang, L., Zielinski, R. J., Qian, W., Wang, Y. A., Mohs, A. M., Kairdolf, B. A., Ji, X., Capala, J., Lipowska, M., Nie, S., Mao, H., & Yang, L. (2019). Targeted Drug Delivery and Image-Guided therapy of heterogeneous ovarian cancer using HER2-Targeted theranostic nanoparticles. *Theranostics*, *9*(3), 778–795.

Schneider, U., Pedroni, E., & Lomax, A. (1996). The calibration of CT Hounsfield units for radiotherapy treatment planning. *Physics in Medicine and Biology*, *41*(1), 111–124. https://doi.org/10.1088/0031-9155/41/1/009

Sebesta, E. M., & Anderson, C. B. (2017). The surgical management of prostate cancer. *Seminars in Oncology*, *44*(5), 347–357.

Shajid, S. M., Aggarwal, L. M., Mourya, A., Choudhary, S., Priean, G., V., Singh, A., & Oommen, S. (2024). A comparison of TG-43 and TG-186 dose calculation algorithms for treatment planning of intra-cavitary brachytherapy using tandem and ovoid applicator. *Journal of Contemporary Brachytherapy*, *16*(4), 289–296. https://doi.org/10.5114/jcb.2024.143138

Sookpeng, S., Cheebsumon, P., Pengpan, T., & Martin, C. (2016). Comparison of computed tomography dose index in polymethyl methacrylate and nylon dosimetry phantoms. *Journal of Medical Physics*, *41*(1), 45. https://doi.org/10.4103/0971-6203.177287

Steiding, C., Kolditz, D., & Kalender, W. (2014). Comparison of methods for acceptance and constancy testing in dental cone-beam computed tomography. *RöFo - Fortschritte Auf Dem Gebiet Der Röntgenstrahlen Und Der Bildgebenden Verfahren*, *187*(04), 283–290. https://doi.org/10.1055/s-0034-1385333

Stish, B. J., Davis, B. J., Mynderse, L. A., McLaren, R. H., Deufel, C. L., & Choo, R. (2018). Low dose rate prostate brachytherapy. *Translational Andrology and Urology*, *7*(3), 341–356.

Su, X., Zhang, G., Xu, S., Qu, W., Song, L., Huang, Y., Wang, B., Wang, Y., Zhang, Z., Xu, W., & Wang, M. (2019). Attenuation coefficients of gamma and X-rays passing through six materials. *Nuclear Science and Techniques*, *31*(1). https://doi.org/10.1007/s41365-019-0717-9

Takácsi-Nagy, Z., Martínez-Mongue, R., Mazeron, J., Anker, C. J., & Harrison, L. B. (2017). American Brachytherapy Society Task Group Report: Combined external beam irradiation and interstitial brachytherapy for base of tongue tumors and other head and neck sites in the era of new technologies. *Brachytherapy*, *16*(1), 44–58.

Taylor, W., Johnson, D., Johnson, M., Ahmad, S., & Chen, Y. (2016). Dosimetric evaluation of tissue heterogeneity for electronic brachytherapy (EBT) source in high dose rate gynecological (GYN) irradiation. *AIP Conference Proceedings*.

Vrbik, I., Van Nest, S. J., Meksiarun, P., Loeppky, J., Brolo, A., Lum, J. J., & Jirasek, A. (2019). Haralick texture feature analysis for quantifying radiation response heterogeneity in murine models observed using Raman spectroscopic mapping. *PloS One*, *14*(2), e0212225.

Wei, Z., Peng, X., Wang, Y., Yang, L., He, L., Liu, Z., Wang, J., Mu, X., Li, R., & Xiao, J. (2021). Influence of target dose heterogeneity on dose sparing of normal tissue in peripheral lung tumor stereotactic body radiation therapy. *Radiation Oncology*, *16*(1).

Williamson, C., Liu, H., Mayadev, J., & Mell, L. (2021). Advances in external beam radiation therapy and brachytherapy for cervical cancer. *Clinical Oncology*, *33*(9), 567–578.

Wu, C. H., Liao, Y. J., Liu, Y. W. H., Hung, S. K., Lee, M. S., & Hsu, S. M. (2014). Dose distributions of An192IR brachytherapy source in different media. *BioMed Research International*, *2014*, 1–11. https://doi.org/10.1155/2014/946213

Xiang, L., Zhang, J., Lin, S., Luo, H., Wen, Q., He, L., Shang, C., Ren, P., Yang, H., Pang, H., Yang, B., He, H., Chen, Y., & Wu, J. (2015). Computed Tomography–Guided Interstitial High-Dose-Rate brachytherapy in combination with regional Positive Lymph node Intensity-Modulated radiation therapy in locally advanced peripheral Non–Small cell lung cancer: a Phase 1 clinical trial. *International Journal of Radiation Oncology, Biology, Physics*, *92*(5), 1027–1034.

Zabihzadeh, M., Yadollahpour, A., & Kargar, L. (2013). The effects of tissue heterogeneitieson dose distribution of iridium-192 source in brachytherapy treatments. *Biomedical & Pharmacology Journal*, *6*(2), 205–213. https://doi.org/10.13005/bpj/404

Zeman, E. M., Schreiber, E. C., & Tepper, J. E. (2020). Basics of radiation therapy. In *Elsevier eBooks* (pp. 431-460.e3). https://doi.org/10.1016/b978-0-323-47674-4.00027-x

Zheng, X., Al-Hayek, Y., Cummins, C., Li, X., Nardi, L., Albari, K., Evans, J., Roworth, E., & Seaton, T. (2020). Body size and tube voltage dependent corrections for Hounsfield Unit in medical X-ray computed tomography: theory and experiments. *Scientific Reports*, *10*(1). https://doi.org/10.1038/s41598-020-72707-y

Zuo, Y., Wei, Y., & Zhu, J. (2018). Influence of beam radius on deposition parameters in dielectric under high energy electron irradiation. *MATEC Web of Conferences*, *189*, 09001.

APPENDICES

ECBAS from University of Ghana for my research

UNIVERSITY OF GHANA
ETHICS COMMITTEE FOR BASIC AND APPLIED SCIENCES (ECBAS)
P. O. Box LG 1195, Legon, Accra, Ghana

Ref. No: ECBAS 111/23-24

7th November, 2024

Mr. Gordon Kwarfo
Department of Medical Physics
University of Ghana
Legon, Accra

Dear Mr. Kwarfo,

ECBAS 111/23-24: EFFECTS OF TISSUE HETEROGENEITIES ON DOSE ESTIMATION IN BRACHYTHERAPY

This is to inform you that the above referenced study has been presented to the Ethics Committee for Basic and Applied Sciences for a full board review and the following actions taken subject to the conditions and explanation provided below:

Expiry Date:	15/09/2025
On Agenda for:	Initial Submission
Date of Submission:	16/07/2024
ECBAS Action:	Approved
Reporting:	Annually

Please accept my congratulations.

Yours sincerely,

INTEGRI PROCEDAMUS

Professor Dorcas Osei-Safo
ECBAS Chairperson

APPENDIX A 1*: HU and rED of tissue inserts within EDP at 80kV*

				HU						
INSERT	TISSUE	ED (×10^23)	rED	1	2	3	4	5	6	AVERAGE
062A-05	Lungs (exhale)	1.632	0.489	-518.36	-482.763	-516.53	-481.19	-510.52	-481.48	-498.474
062A-06	Breast	3.261	0.976	-56.53	-44.55	-52.12	-43.99	-48.72	-45.09	-48.5
062A-10	Muscle	3.483	1.043	56.88	44.74	57.25	50.62	55.9	53.76	53.19167
062A-04	Lungs (inhale)	0.634	0.19	-845.57	-811.17	-844.92	-817.17	-844.13	-826.79	-831.625
062A-15	Bone 800g/cc	4.862	1.456	1282.74	1219.09	1284.22	1225.68	1275.47	1227.31	1252.418
062A-08	Bone 200g/cc	3.73	1.117	325.59	335.49	328.78	343.21	328.46	350.37	335.3167
062A-09	Liver	3.516	1.053	46.31	81.14	41.81	81.86	39.41	82.72	62.20833
062A-11	Adipose	3.17	0.949	-87.67	-41.78	-86.75	-45.18	-84.11	-47.72	-65.535
062AMA-39	Water	3.34	1	4.76		2.19		9.73		5.56

APPENDIX A 2*: HU and rED of tissue insert within EDP at 100k*

EDP-100kv				HU						
INSERT	TISSUE	ED (×10^23)	rED	1	2	3	4	5	6	AVERAGE
062A-05	Lungs (exhale)	1.632	0.489	-497.66	-495.33	-497.08	-494.82	-496.14	-496.99	-496.337
062A-06	Breast	3.261	0.976	-36.23	-32.32	-35.97	-30.55	-35.47	-32.3	-33.8067
062A-10	Muscle	3.483	1.043		40.15	44.1	41.54	44.61	42.4	42.56
062A-04	Lungs (inhale)	0.634	0.19	-831.75	-830.63	-833.29	-827.43	-831.49	-826.98	-830.262
062A-15	Bone 800g/cc	4.862	1.456	1009.75	995.97	1010.16	997.92	1014.73	998.22	1004.458
062A-08	Bone 200g/cc	3.73	1.117		258.66	267.38	259.65	268.43	261.4	263.104
062A-09	Liver	3.516	1.053	51.28	49.81	51.66	51.89	51.63	51.73	51.33333
062A-11	Adipose	3.17	0.949	-71.12	-71.47	-69.83	-70.78	-69.58	-70.12	-70.4833
	Water	3.34	1	-22.05		-22.44		-20.52		-21.67

APPENDIX A3*: HU and rED of tissue insert within EDP at 120kV*

EDP-120kV				HU						
INSERT	TISSUE	ED (×10^23)	rED	1	2	3	4	5	6	AVERAGE
062A-05	Lungs (exhale)	1.632	0.489	-497.9	-496.33	-496.6	-495.12	-495.49	-491.1	-495.423
062A-06	Breast	3.261	0.976	-33.15	-30.33	-29.73	-26.85	-16.76	-11.23	-24.675
062A-10	Muscle	3.483	1.043	40.37	37.01	41.73	40.23	46.39	54.17	43.31667
062A-04	Lungs (inhale)	0.634	0.19	-826.11	-825.01	-831.84	-828.99	-836.58	-841.49	-831.67
062A-15	Bone 800g/cc	4.862	1.456	872.01	861.64	874.5	861.39	885.17	870.16	870.8117
062A-08	Bone 200g/cc	3.73	1.117	233.34	224.83	232.95	224.46	241.26	236.37	232.2017
062A-09	Liver	3.516	1.053	50.62	48.32	51.09	49.19	51.28	55.94	51.07333
062A-11	Adipose	3.17	0.949	-63.72	65	-63.77	-63.54	-63.4	-60.52	-41.6583
	Water	3.34	1	-21.24		-24.9		-10.5		-18.88

APPENDIX A 4*: HU and rED of tissue insert within EDP at 140kV*

EDP-140kV						HU				
INSERT	TISSUE	ED (×10^23)	rED	1	2	3	4	5	6	AVERAGE
062A-05	Lungs (exhale)	1.632	0.489	-494.27	-492.13	-494.37	-493.81	-495.4	-492.96	-493.823
062A-06	Breast	3.261	0.976	-27.37	-26.1	-29.51	-27.37	-28.71	-25.84	-27.4833
062A-10	Muscle	3.483	1.043	41.55	37.43	41.58	37.36	40.88	37.14	39.32333
062A-04	Lungs (inhale)	0.634	0.19	-826.09	-822.94	-823.31	-824.49	-824.75	-822.01	-823.932
062A-15	Bone 800g/cc	4.862	1.456	790.97	780.34	792.54	780.92	792.1	780.41	786.2133
062A-08	Bone 200g/cc	3.73	1.117	210.96	202.59	210.21	203.87	210.21	203.28	206.8533
062A-09	Liver	3.516	1.053	49.99	48.47	50.09	46.63	49.79	47.04	48.66833
062A-11	Adipose	3.17	0.949	-59.9	-60.75	-60.5	-61.03	-59.9	-60.52	-60.4333
062A-39	Water	3.34	1	-20.82		-18.9		-20.47		-20.0633

APPENDIX B1: HU, ED and rED of selected materials at 80kV

EDP 80kV				HU						
INSERTS	MATERIAL	ED (×10^23)	rED	1	2	3	4	5	6	AVERAGE
062A-08	FRYTOL	3.405	1.036	2.066254	317.74	-138.77	319.44	-143.18	329.34	114.43938
062A-09	NaOH	3.416	1.049	0.41509	50.96	148.7	50.16	143.58	55.62	74.905848
062A-11	SAE15-40	3.011	0.911	0.163185	-82.85	-143.44	-82.56	-142.81	-75.79	-87.881136
062A-05	AIR	2.016	0.064	-469.83	-462.52	-455.94	-455.1	-454.1	-452.54	-458.255

APPENDIX B1: HU, ED and rED of selected materials at 100kV

EDP100kV				HU						
INSERTS	MATERIAL	ED (×10^23)	rED	1	2	3	4	5	6	AVERAGE
062A-08	FRYTOL	3.508	1.036	-119.99	260.57	-119.47	259.49	-119.28	260.39	70.285
062A-09	NaOH	3.55	1.049	150.17	49.94	150.82	50.19	150.25	50.26	100.272
062A-11	SAE15W-40	3.046	0.911	-129.68	-70.1	-128.26	-71.31	-129.57	-72.33	-100.208
062A-05	AIR	1.755	0.525	-495.23	-488.28	-481.2	-466.67	-480.0	-467.9	-479.88

APPENDIX B1: HU, ED and rED of selected materials at 120kV

EDP 120kV						HU				
INSERTS	MATERIAL	ED (×10^23)		1	2	3	4	5	6	AVERAGE
062A-08	FRYTOL	3.499	1.036	-108.65	228.43	-107.81	228.1	-114.39	226.01	58.615
062A-09	NaOH	3.566	1.049	149.54	50.14	148.06	50.06	140.65	49.39	97.9733
062A-11	SAE15-40	3.042	0.911	-118.69	-62.91	-118.15	-63.68	-117.74	-63.23	-90.733
062A-05	AIR	1.754	0.525	-476.6	-466.32	-476.63	-466.19	-500.65	-499.69	-481.013

APPENDIX B1: HU, ED and rED of selected materials at 120kV

EDP 140kV				HU						
INSERTS	MATERIAL	ED (×10^23)		1	2	3	4	5	6	AVERAGE
062A-08	FRYTOL	3.434	1.036	-104.25	204.22	-102.01	204.93	-102.74	2O5.56	20.03
062A-09	NaOH	3.485	1.049	-144.43	47.97	145.82	48.63	141.9	49.35	48.206667
062A-11	SAE15-40	3.076	0.911	-113.12	-59.74	-112.4	-59.02	-113.75	-58.5	-86.088333
062A-05	AIR	1.784	0.534	-491.79	-479.47	-468.84	-443.03	-468.91	-443.12	-465.86